Multivalent Interactions between Molecular Components Involved in Clathrin Independent Endocytosis Drive Protein Phase Separation

Samsuzzoha Mondal, Samuel Botterbusch, Karthik Narayan, Imania Powers, Jason Zheng, Rui Jin, and Tobias Baumgart*

Department of Chemistry, University of Pennsylvania, Philadelphia, Pennsylvania, 19104, United States.

* To whom correspondence may be addressed. Email: baumgart@sas.upenn.edu

Abstract

Endocytosis of transmembrane receptors initiates via molecular interactions between the activated receptor and the endocytic machinery. A specific group of receptors, including the β1-adrenergic receptor (β1-AR), is internalized through a non-clathrin pathway known as Fast Endophilin Mediated Endocytosis (FEME). A key question is: how does the endocytic machinery assemble and how is it modulated by activated receptors during FEME. Here we show that endophilin, a major regulator of FEME, undergoes a phase transition into liquid-like condensates, which facilitates the formation of multi-protein assemblies by enabling the phase partitioning of endophilin binding proteins. The phase transition can be triggered by specific multivalent binding partners of endophilin in the FEME pathway such as the third intracellular loop (TIL) of the β1-AR, and the proline-rich-motifs of lamellipodin (LPD-PRMs). Other endocytic accessory proteins can either partition into, or target interfacial regions of, these condensate droplets. On the membrane, TIL promotes protein clustering in the presence of endophilin and LPD-PRMs. Our results demonstrate how the multivalent interactions between endophilin, LPD-PRMs and TIL regulate protein assembly formation on the membrane, providing mechanistic insights into the priming and initiation steps of FEME.

Introduction

Endocytosis is an essential cellular process, such as for maintaining transmembrane receptor homeostasis at the cell surface (1-4). Endocytic pathways require the local recruitment of adapter proteins at the membrane to form transport carriers, followed by sequestration of the receptors into them (5-7). Most adapter proteins contain a lipid binding domain for membrane anchoring as well as additional domains to interact with one or more protein binding partners. Functionality of these proteins is regulated by coincidence detection of their binding partners and specific membrane lipids (8-11). The nature and strength of these molecular interactions play a crucial role in the dynamic assembly and disassembly of endocytic complexes at the plasma membrane.

Clathrin mediated endocytosis (CME) is the dominant uptake pathway in eukaryotes but various clathrin independent endocytosis (CIE) pathways exist in parallel that are either cargo-specific or are activated by specific cellular conditions such as receptor hyperstimulation and stress response (12,13). Fast endophilin mediated endocytosis (FEME) is a recently discovered CIE pathway that allows rapid uptake of a subset of G-protein coupled receptors (GPCRs), and receptor tyrosine kinases (13-15). The β1-adrenergic GPCR (β1-AR) is exclusively internalized via FEME (14). Endophilin, a Bin/Amphiphysin/Rvs (BAR) domain protein plays a central role in FEME by driving cargo capture and subsequent generation of membrane curvature during FEME. The multifunctionality of endophilin is enabled by its two functional domains – the BAR domain interacts with the membrane and the Src homology 3 (SH3) domain binds to specific target proteins that contain proline-rich-motifs (PRMs) (14,16,17). FEME requires pre-enrichment of endophilin on the plasma membrane in the form of transient patches formed with the help of an adapter-protein called lamellipodin (LPD). Receptor activation further allows endophilin patch interactions with the receptors' PRM-rich third intracellular loop (TIL). At a key step in FEME, TIL binding of endophilin is known to be crucial for receptor internalization (13). The TIL-endophilin interaction has been suggested to catalyze membrane curvature generation during FEME (13,15). However, the exact molecular mechanism of how TIL-endophilin interactions facilitate the FEME pathway, is still unclear.

Multivalency is often found to contribute to PRM domain containing protein interactions with SH3 domain containing proteins (18-20). Endophilin exhibits a bivalency since it exists as homodimer in solution. This bivalency can be amplified through oligomerization after endophilin binds to the membrane (21,22). Furthermore, the C-terminal domain of LPD and the TIL region of GPCRs contain multiple PRMs that can interact with endophilin. Multivalent interactions between proteins can lead to liquid-liquid phase separation (LLPS) resulting into a condensed phase coexisting with a dilute aqueous phase (19). In cells, LLPS drives formation of membrane organelles and also has implications in the clustering of signaling molecules on the plasma membrane (23-25). Actin signaling proteins Nck and N-WASP that contain multiple SH3 and PRMs exhibit a now classic example for LLPS driven by multivalent interactions (19). In signaling complexes, LLPS can facilitate sharp transitions in protein functionality by enhancing the local concentration of proteins (18,20,25,26). In CME, LLPS has been suggested to serve a principal mechanism to enhance protein assembly. A recent study by Day *et al.* reported that LLPS driven by multivalent interactions between FCho1/2 and Eps15 catalyzes the initiation of CME. Here we asked, if similar multivalent interactions between endophilin and its multi-PRM binding partners can lead to LLPS. Specifically, we hypothesized that LLPS promotes formation of dynamic endophilin rich clusters on the membrane that could function as priming sites for FEME. The liquid-like clusters could then recruit additional endocytic proteins, such as the activated receptor. Enhanced protein activity at the membrane due to increased local concentrations would then eventually lead to formation of FEME transport carriers.

In this study, we set out to determine under what conditions endophilin and PRM domain containing proteins undergo LLPS. We found that endophilin on its own forms liquid-like droplets in bulk solution in the presence of molecular crowding agents. The droplets enabled the partitioning of various endophilin binding proteins to be studied. These proteins functioned to either promote or suppress the phase separation. More importantly, endophilin underwent LLPS in bulk solutions even in the absence of crowding agents upon binding to its two major interaction partners in the FEME pathway – 1) TIL of the β1-AR (14) and 2) a synthetic tandem multimer of PRM (PRM7), considered as a rough model for the

disordered C-terminal domain of LPD. We further showed that on a lipid bilayer with reconstituted TIL, PRM7, and endophilin form protein clusters through two-dimensional phase separation. Interestingly, we observed that endophilin has a higher propensity to cluster with TIL than with PRM7 on the membrane suggesting that TIL, by catalyzing LLPS, can initiate the formation membrane transport carriers. Altogether, our findings suggest that LLPS could be key mechanism in the formation of protein assembly in FEME by permitting rapid sorting of activated GPCRs into endophilin rich clusters to form transport carriers.

Results

Endophilin alone undergoes LLPS in crowded environment

We first set out to investigate whether BAR-proteins can undergo LLPS by self-interactions under physiological conditions. Over 80% of the proteins in human proteome are predicted to undergo LLPS either spontaneously or under suitable conditions (27). The BAR superfamily proteins are well known for their ability to oligomerize on membranes. (28-30). There has been no evidence thus far of BAR-proteins undergoing LLPS exclusively through self-interactions. In the cellular environment, macromolecular crowding generates an excluded volume effect that is known to promote LLPS in various proteins by shifting the boundary of phase transition toward lower threshold protein concentrations (31-33). To test if molecular crowding can promote LLPS in the N-BAR protein endophilin, we introduced the protein (A1 isoform of endophilin, from rat) to a solution containing 10% (w/v) polyethylene glycol (PEG, average molecular weight 8000 Da), a polymeric crowding agent that is commonly used to mimic the cellular crowding environment *in vitro* (34). Endophilin was observed to form micron sized liquid-like droplets at concentrations of 10 μM and higher. Formation of liquid droplets was confirmed by their spherical appearances under transmitted light microscopy **(Figure 1A)**. Confocal fluorescence images recorded in the presence of Alexa 594-labeled endophilin (4 mol%) along with unlabeled endophilin (25 μM) showed ~70 times brighter intensities than the droplets compared to the bulk solution demonstrating that the droplets are indeed protein condensates **(Figure 1A)**. We constructed a phase diagram by mixing various

concentrations of endophilin at different PEG concentrations at room temperature and examining the solution for the presence of liquid-like droplets by transmitted light imaging **(Figure 1B)**. Lowering PEG concentration from 10% to 2.5% increased the threshold endophilin concentration for LLPS from 10 µM to 90 µM. The observed PEG dependence of LLPS boundary is consistent with the notion that molecular crowding promotes phase separation as observed in a variety of different proteins (31-33).

The liquid-like state is typically metastable and protein condensates can further undergo liquid-to-gel like transitions by establishing long-lived intermolecular interactions (35,36). That transition is generally facilitated by the presence of crowding agents and results in reduced protein mobility within the droplets (37). We assessed the translational mobility of Alexa 488 labeled endophilin (4 mol% out of total endophilin protein) within the droplets at various concentrations of PEG by fluorescence recovery after photobleaching (FRAP) measurements (**Figure 1C**). The fluorescence recovery profiles were best fit by a double-exponential model for 2.5-7.5% PEG and a single-exponential model for 10% PEG (**Figure 1D)**. The droplets showed partial photorecovery suggesting the presence of both liquid-like and gel-like features in the droplets (37,38). The fraction of the protein in the mobile state (mobile fraction) reduced from 80% to 30% between 5% and 10% PEG suggesting that the liquid-to-gel transition shows a significant PEG concentration dependence at this range **(Figure 1E)**. Interestingly, the average halftime ($t_{1/2}$) of photorecovery obtained from the exponential fits did not vary significantly at different PEG concentrations (*Supplementary Figure 1*). This observation suggests that endophilin rich droplets transition into a biphasic state consisting of a mobile phase with unchanged diffusion properties and a second, solid-like phase where the protein is immobilized.

Transition from liquid to gel-like states in proteins are often associated with misfolding and the formation of amyloid structures (32,33,39). To test if the gel-like transition in endophilin also occurs via protein conformation changes, we performed circular dichroism (CD) in the presence and absence of 10% PEG (*Supplementary figure 2A*). CD spectra recorded at a protein concentration of 5 µM which is below the threshold for LLPS (10 µM) did not show significant differences in the spectral features in the presence

or absence of PEG. Above the LLPS threshold (20 μM), the helical features of the spectra remained similar but an overall loss in CD signal intensities at all wavelengths was observed in the presence of PEG, likely caused by a loss in protein concentration in solution due to settling of some droplets (*Supplementary figure 2B*).

We observed fast gelation kinetics on a minute time scale for endophilin droplets as indicated by our FRAP studies. About 70% of the protein had matured to a gel-like state within 10 minutes of mixing the protein with 10% PEG. The timescale of the liquid-to-gel transition is believed to be protein sequence dependent. Under similar conditions (10% PEG), droplets formed by α-synuclein undergo a gel-like transition at much slower rate that occurred over a time course of days whereas the transition in β-synuclein takes place at a minute time scale like that observed for endophilin (33). Reducing the PEG concentration to 5% resulted in relatively slower gelation kinetics and we could observe a significant drop in the mobile fractions between measurements taken within 10 min and 30 min after mixing. This fraction did not change significantly when monitored over the course of 21 hours indicating that the endophilin droplets reach maturation within an hour of formation *(Supplementary figure 3)*. Fast transition of endophilin droplets into a gel-like state without showing conformation changes suggests that the protein molecules rapidly reorganize themselves to form strong association after forming liquid droplets.

LLPS is driven by the BAR domain itself

With the aim to understand molecular mechanisms behind endophilin self-oligomerization, we asked what functional domains of endophilin are the main drivers for LLPS (**Figure 1F**). Cryo-electron microscopy has revealed that endophilin oligomers formed on membrane nanotubes are stabilized by interactions between H0 helices from adjacent N-BAR domains (21). In addition, the H0 helix is also known to interact with the SH3 domain in solution in the homodimeric form of endophilin (40,41), We hypothesized that, under suitable conditions H0-H0 and H0-SH3 interactions may lead to crosslinking between the endophilin dimers that can lead to oligomerization. To test whether H0 helix mediated interactions promote LLPS, we generated a mutant lacking the H0 helix (ΔH0). However, the ΔH0 mutant also formed droplets in the

presence of PEG and the threshold concentration of droplet formation was comparable (7 μM) to that of the full-length protein (10 μM) (**Figure 1F**). This indicates that the H0 helix has moderate to no contribution to the LLPS. We further asked whether LLPS in endophilin is promoted by its 45 amino acid long (aa 248-292), intrinsically disordered linker region that exists between the N-BAR domain and SH3 domain. An endophilin mutant lacking the N-BAR domain (ΔN-BAR, comprising the SH3 domain and its disordered linker) did not form droplets even at the concentration of 70 μM in the presence of 10% PEG (**Figure 1F)**. Strikingly, an N-BAR-only mutant of endophilin, lacking both the linker and the SH3 domain, formed liquid-like droplets even at a lower threshold concentration (5 μM) than the full-length protein (**Figure 1F**, *Supplementary Figure 4*. These observations implicated that, rather than interactions between different types of domains of the endophilin protein, the self-association behavior specifically of the BAR domain scaffold, drives LLPS in endophilin.

The fact that the N-BAR only mutant shows LLPS at the lowest concentration (**Figure 1F**) indicated that either the disordered linker or the SH3 domain might suppress droplet formation in the full-length protein. One possibility could be that the disordered linker, via steric effects, interferes with the self-assembly of the N-BAR domains. This notion was further supported by the observation that full length amphiphysin, which contains a much longer (383 aa) disordered linker than endophilin (45 aa), did not form liquid-like droplets in the presence of 10% PEG up to a protein concentration of 60 μM (Supplementary Figure 5). To further test the hypothesis of an LLPS inhibition effect of BAR protein linkers, we purified an N-BAR-only mutant of amphiphysin and introduced it to 10% PEG. Notably, the N-BAR only mutant of amphiphysin formed droplets associated with an LLPS boundary (2 μM) that was comparable with the endophilin N-BAR. This observation strongly indicates that the disordered linker can play an inhibitory role in the N-BAR domain driven LLPS. Overall, the discovery of LLPS phenomena in the N-BAR proteins could provide new mechanistic insights into BAR protein mediated membrane remodeling and formation of protein assembly in endocytic pathways.

We further compared the relative tendencies of full length endophilin and the mutants to be in the condensed phase over the dilute phase at a fixed concentration of PEG. With the assumption that Alexa 594 labeled proteins would have similar partitioning abilities as the unlabeled proteins between the condensed and the dilute phases, a minor amount (4 mol%) of labeled proteins was added to unlabeled full length protein, ΔH0 mutant, and N-BAR-only mutant prior to droplet formation. This enabled estimation of the relative protein densities of the two phases from the ratio of the fluorescence intensities inside and outside droplets. The ratios were similar for full length endophilin and ΔH0 (480 ±60 and 380 ±100 respectively), whereas it was significantly higher (1800 ±400) for the N-BAR-only mutant (**Figure 1G**). A larger density of the N-BAR domain in the condensed phase compared to full length protein is consistent with the notion that the BAR domain has higher phase separation tendency compared to the full-length protein, as indicated by its phase separation at a lower threshold protein concentration. To test whether this contribution comes from any specific interaction between the SH3 domain and other functional domains of the protein, we estimated tendencies of the SH3 domain itself to partition into the droplets full length protein and the two other mutants (*Supplementary figure 6*). Partition coefficients for Alexa 594 labeled SH3 domain were similar and in between 7-12 for all three types of droplets, suggesting that the SH3 domain contributes minimally to the partitioning of endophilin into droplets.

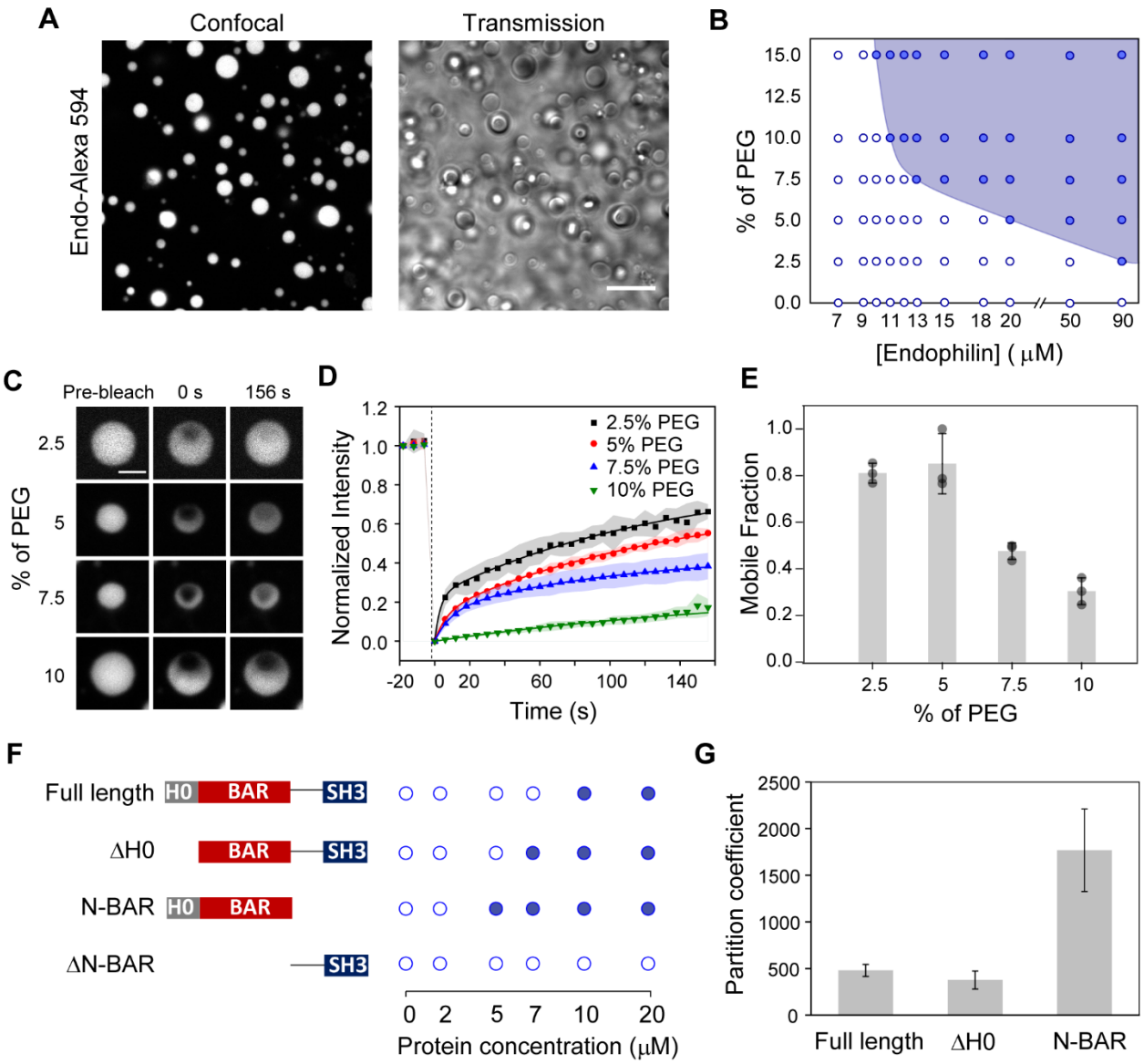

Figure 1: Endophilin undergoes LLPS in crowded environment. A. Droplets formed by rat endophilin A1 (25 µM) in the presence of 10% PEG. Left, confocal fluorescence image of LLPS droplets of endophilin doped with Alexa 594-labeled endophilin (1 µM); right, transmission image of the droplets. Scale bar 10 µm. **B.** Phase diagram showing endophilin-PEG LLPS system. The filled circles indicate where liquid-like droplets were observed whereas the open circles indicate no droplet formation. **C.** Representative confocal images of endophilin droplets before, 0 s after, and 200 s after photobleaching at different PEG concentrations. **D.** FRAP time profiles to show the recovery rate at different PEG concentrations. Normalized intensities of bleached area relative to the unbleached intensities are plotted for each time point. Each data point is an average of three repeats performed on different droplets, error bars indicate standard deviation. The solid lines indicate 2-exponential (2.5%, 5%, and 7.5% PEG) or 1-exponential (10% PEG) fits of the recovery profiles. **E.** Bar plot showing the mobile fractions of protein within the droplets obtained from the exponential fits of the recovery profiles. Error bars indicate standard deviations of three independent FRAP profiles. **F.** Domain structures of full length endophilin, its ΔH0 mutant, N-BAR only mutant, and ΔN-BAR mutant and their phase behavior in the presence of 10% PEG. All three forms start showing LLPS between 5 to 10 µM protein concentrations. The filled circles indicate liquid-like droplets were observed whereas the open circles indicate no droplet formation. **G.** Bar plot showing the partition

coefficients for Alexa 594 labeled endophilin variants into corresponding droplets. Data is presented as mean±s.d. *N* = 11-20 droplets.

Binding partners of endophilin partition into LLPS droplets

A protein undergoing LLPS can sequester binding partners as 'clients' where the host protein is termed 'scaffold' (42). Relative partitioning tendencies of various clients into a scaffold can be compared via their apparent partition coefficient (K_{app}) values (43). Endophilin interacts with various binding partners in the CME and FEME pathways. The interactions are mainly mediated by the SH3 domain of endophilin which binds to target PRM containing proteins (14,44). While LLPS in endophilin was found to be driven by mainly through the N-BAR domain, the SH3 domain can promote sequestration of PRM containing proteins into the droplets. We hypothesize that phase separation of endophilin facilitates formation of endocytic protein assembly by allowing partitioning of other endocytic proteins as clients **(Figure 2A)**.

We first tested the partitioning abilities of two potential clients of endophilin in the FEME pathway. One of these was the 80 amino acid long TIL region of the β1-adrenergic receptor (aa 246-325) which is intrinsically disordered and contains several PxxP motifs (where P is proline, x is any amino acid) which are known to bind endophilin SH3 (14,17). The second client we considered was the C-terminal domain of LPD. The entire C-terminal domain of LPD is a 658 amino acid long (aa 593-1250) disordered sequence that contains 10 PRMs, each 12-13 amino acids long. These PRMs have been shown to bind the endophilin SH3 domain (16). To facilitate purification, we designed a relatively shorter (177 amino acid long) synthetic mimic of the LPD C-terminal domain that consists of a heptameric repeat of a single PRM (aa 970-981) connected by flexible $(Gly\text{-}Gly\text{-}Ser)_4$ linkers (PRM7). Fluorescently labeled TIL and PRM7 were mixed (4 mol%) with unlabeled endophilin prior to inducing LLPS by adding of PEG (10%). TIL and PRM7 showed much brighter fluorescence intensities from the droplet phase compared to the bulk phase indicating they both partition into droplets as clients **(Figure 2B)**. The K_{app} value for TIL and PRM7 (140±40 and 26±4 respectively) indicated both peptides partition strongly into endophilin droplets, where TIL showed 5 times stronger partitioning than PRM7 **(Figure 2C)**. Partitioning of these binding partners of endophilin into the

condensed phase via 'scaffold-client' interaction might constitute a key mechanism behind protein sorting in FEME.

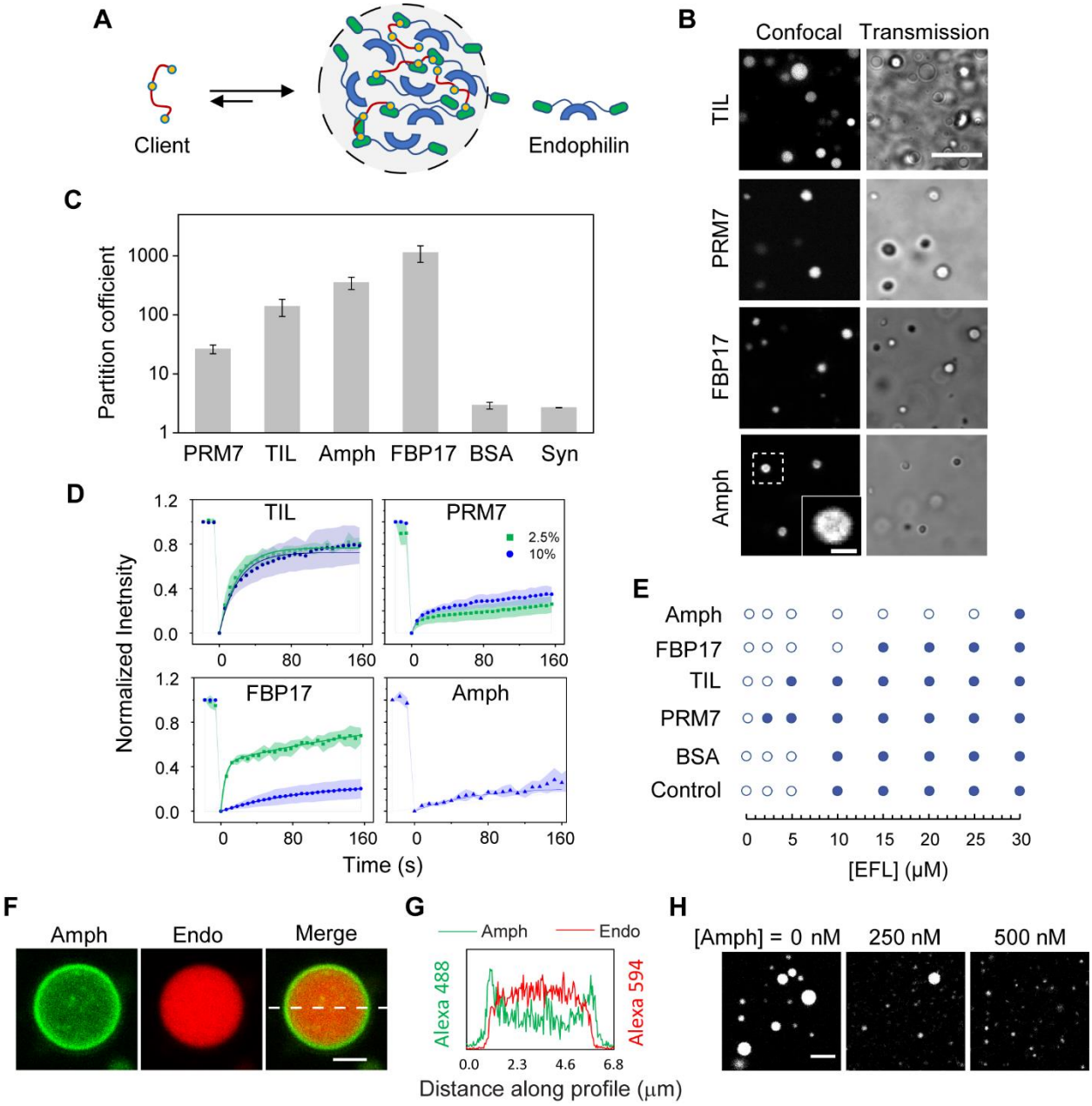

Figure 2: Endophilin binding partners partition into LLPS droplets and exhibit regulatory behavior. **A.** Graphical illustration of endophilin droplet formed by LLPS allowing partitioning of endophilin binding proteins as clients into the condensed phase. **B.** Confocal images showing partitioning of fluorescently labeled TIL (Alexa 488) of β1-adrenergic receptor, PRM7 (Alexa 633) of lamellipodin, FBP17 (Alexa 488) and amphiphysin (Alexa 488) into droplets formed by endophilin in the presence of 10% PEG. The corresponding transmission images show the endophilin droplets. Scale bar 10 µm. In the case of amphiphysin, an enlarged image is shown in the inset (scale bar 2 µm) for the droplet surrounded by dotted lines to illustrate the peripheral distribution of the protein. **C.** Partition coefficients for the clients within

endophilin droplets as determined from fluorescence intensities inside and outside the droplets. **D**. FRAP profiles of the client proteins partitioned within endophilin droplets formed in the presence of 2.5% and 10% PEG. **E.** Effect of client proteins on the endophilin-PEG phase boundary. **F.** Peripheral distribution of amphiphysin within endophilin droplets. **G.** Fluorescence intensity profile along the dotted white line showing amphiphysin-Alexa 488 fluorescence intensity is higher along the edges of the droplet. **H.** Confocal images of endophilin droplets formed in the presence of 10% PEG and various concentrations of amphiphysin.

In addition to the two major peptide-based clients, we tested partitioning of two BAR proteins, amphiphysin 1 and FBP17, that are functionally linked to endophilin in CME and CIE pathways. Amphiphysin 1 was reported to interact with the SH3 domain of endophilin *in vitro* via PRMs present at its large disordered linker region and this interaction has been implicated in CME of synaptic vesicles (45,46). FBP17 is involved in regulating recruitment of LPD during FEME and is also shown to co-localize with endophilin at sites of CME (47) (48). Both amphiphysin and FBP17 strongly partitioned into the droplets. Interestingly, amphiphysin showed an anisotropic partitioning behavior by accumulating more at the droplet periphery than the interior. The K_{app} values were 350 ±80 and 1130 ±350 for amphiphysin and FBP17 respectively indicating their high propensities to form assembly with endophilin scaffolds during endocytosis (**Figure 2C**). We caution that the ability of partitioning into droplets does not always imply existence of specific scaffold-client interactions since protein partitioning into the condensed phase can also be driven by weak, non-specific interactions (42,43). Accordingly, we further asked, to what extent specific scaffold-client interactions contribute to the client partitioning. To begin to address this, we tested partitioning of a folded and an intrinsically disordered protein, BSA and α-synuclein that do not have any specific interaction with endophilin. Both BSA and α-synuclein partitioned into endophilin droplets to a much weaker extent showing K_{app} values of ~ 3 strongly suggesting that the protein partitioning into droplets is mainly favored by specific scaffold-client interactions **(Figure 2C).** These results illustrate the importance of specific protein-protein interactions in the formation of LLPS driven protein assembly in the endocytic pathway.

We then aimed to explore whether the transition of the scaffold into the gel-like phase affects client mobility within droplets. TIL and PRM7 were allowed to partition into droplets formed in the presence 2.5% and 10% PEG and their FRAP profiles were monitored. Interestingly, the recovery profiles for both TIL and PRM7 were PEG independent **(Figure 2D)**. However, TIL showed a greater extent of recovery (90% mobile fraction) than PRM7 (50% mobile fraction) indicating that PRM7 might interact stronger with endophilin in the droplet phase, perhaps due to PRM7's higher valency than TIL's. A reason why the disordered peptide clients did not show a PEG dependence in their mobility could be that pores of the gel-like network allow greater mobility of the flexible macromolecules than rigid, folded proteins (49) such the diffusion behavior of the peptides in the gel-like phase is comparable to that in the liquid-like phase. In contrast to the peptide clients, the protein clients showed a PEG concentration dependent mobility within the droplets. FBP17 showed faster recovery and larger mobile fraction at 2.5% PEG compared to 10% PEG indicating that mobility of FBP17 is significantly restricted by the gel-like state in endophilin **(Figure 2D)**. Interestingly, droplets formed at 2.5% PEG in the presence of amphiphysin were too small to perform FRAP. This small size would be consistent with an inhibitory role of amphiphysin in the formation of larger droplets. However, in the presence of 10% PEG, the droplets were large enough to be able to perform FRAP and the photorecovery profile of amphiphysin was comparable to that of FBP17 **(Figure 2D)**. To summarize, endophilin binding partners displayed protein specific partitioning behavior. We next investigated the phase boundary regulating behavior of these proteins.

<u>Clients can act as regulators of the LLPS depending on their molecular features</u>

Clients partitioning into the droplet phase can significantly perturb scaffold-scaffold interactions and hence the clients can act as regulators of LLPS. (43). To capture the regulatory behavior of the endophilin binding partners on the phase boundary, we determined the threshold endophilin concentration for LLPS (with 10% PEG) in the presence of a fixed client concentration (10 μM) (**Figure 2E**). Both TIL and PRM7 were found to promote endophilin phase separation as the threshold was shifted from 10 μM to 5 μM in the presence of TIL and to 2 μM in the presence of PRM7. Amphiphysin was found to suppress optically resolvable

LLPS. The presence of amphiphysin increased the threshold concentration for droplet formation 3-fold (from 10 µM to 30 µM) whereas FBP17 had a more moderate effect on the threshold (15 µM). As expected, the phase boundary remained unchanged in the presence of the weakly partitioning client BSA, reassuring that the regulatory roles exhibited by the clients are dependent on their abilities to form specific interactions with the scaffold. We discuss the role of amphiphysin in modulating droplet size through interfacial droplet partitioning (50) further below.

It is noteworthy that the partitioning tendencies of TIL and amphiphysin do not differ significantly (K_{app} values 54±21 and 81±17 respectively) yet they show reverse regulatory behavior on the LLPS. Earlier, it was observed that the regulators influence LLPS depending on their partitioning abilities into the host protein (43). Our study further shows that with strongly partitioning clients, molecular features of the client itself and specific interactions between the client and the host proteins could be two major deciding factors in the regulatory action of the client protein. The promotion of LLPS by endophilin in the presence of TIL and PRM7 could be attributed to their abilities to form multivalent interactions with the scaffold protein, endophilin. In case of amphiphysin, the large, disordered region that we proposed to inhibit LLPS in amphiphysin itself, might suppress LLPS of endophilin by weakening scaffold-scaffold interactions, when these two proteins bind to each other.

Amphiphysin forms solid-like shell and suppresses LLPS of endophilin

We further queried how the suppression of LLPS in the presence of amphiphysin is related to its unique, anisotropic partitioning behavior into endophilin droplets (**Figure 2C**). While Alexa 488 labeled amphiphysin showed a higher fluorescence intensity at the droplet periphery compared to the central region, the distribution of endophilin remained homogeneous, as verified from the intensity distribution of Alexa 594 labeled endophilin within the droplets (**Figure 2F, 2G)**. FRAP performed on the peripheral region of the droplets showed no photorecovery suggesting that amphiphysin forms a solid-like shell around the droplets (*Supplementary figure 7*). Solid-like shell formation has been reported in multicomponent protein droplets including recently observed intranuclear droplets where RNA-binding protein TDP-43 forms solid

shells around a liquid-like core formed by HSP40 family chaperones (51). Anisotropic distribution of molecular components in multiphase condensates has been attributed to favorable solvent interaction of the shell component over the core components that results into decrease in surface tension of the overall system (52,53). Interestingly, the N-BAR domain of amphiphysin showed a homogeneous partitioning (*Supplementary figure 8A*) indicating that the anisotropic distribution of the protein within endophilin droplets is most likely driven by the disordered linker and the SH3 domain. Recently, amphiphilic proteins containing a condensed phase-liking part in addition to a dilute phase-liking part have been shown to form a similar shell-like layer on condensate surfaces (50). Such amphiphilic proteins, having surfactant like properties, have been shown to regulate the size of biomolecular condensates (50). Indeed, we observed a significant drop in the number of the large droplets (1 µm or above) formed by endophilin (25 µM protein, 10% PEG) in the presence of 0.1-1 µM of amphiphysin **(Figure 2H,** and *Supplementary figure 8B***)**. Above 1 µM of amphiphysin, the total number of endophilin droplets decreased significantly and no droplets were observed above 2 µM amphiphysin (*Supplementary figure 8C*). The observed amphiphilic, surfactant-like properties suggests a potential role of amphiphysin as a size regulator of endocytic protein assemblies.

Endophilin undergoes LLPS upon interactions with multiple PRM containing ligands even in the absence of a crowding agent

Having observed inherent abilities of endophilin to undergo LLPS in crowded environments and promotion of the LLPS by its multivalent binding partners, TIL and PRM7, further encouraged us to test whether these two binding partners can drive LLPS in endophilin even in the absence of a crowding environment. We therefore mixed various concentrations of endophilin with equimolar concentrations of either TIL or PRM7. With TIL we observed formation of tiny (submicron size) droplets beginning at 20 µM and micron size droplets above 75 µM protein concentration, which implies endophilin TIL interactions drive macroscopic protein-protein phase separation (**Figure 3B)**. With PRM7, droplet formation began at 10 µM protein concentration. In solution, the droplets coalesced to form larger droplets in a few minutes. Upon settling on glass coverslips, droplets were found to wet (i.e. spread on) the glass surface within 10 min. To check

protein mobility within the droplets we performed FRAP on both endophilin and the peptide components. TIL and PRM7 showed rapid photorecovery ($t_{1/2}$ 2 s and 0.3 s respectively) compared to endophilin in both cases ($t_{1/2}$ 21 s and 17 s respectively) (**Figure 3C, 3D)**. TIL and PRM7 also showed larger mobile fractions (70-80%) than endophilin (35%). A reduced fractional mobility is indicative of the formation of a gel-like state via N-BAR domain driven self-association that we had observed in the case of droplets formed in the presence of PEG (**Figure 1**). This implies that the N-BAR domain driven self-interaction can still take place within droplets formed by multivalent SH3-PRM interactions.

Phase diagrams for both endophilin-TIL and endophilin-PRM7 systems were constructed by mixing endophilin and the peptides at various molar ratios and concentrations (**Figure 3E, 3F**). The phase boundary for equimolar mixing was found to be 20 µM for the endophilin/TIL system and 10 µM for the endophilin/PRM7 system. A lower phase boundary with PRM7 is consistent with its slightly stronger ability in shifting the endophilin LLPS boundary (with 10% PEG) compared to TIL. Our previous observation that TIL and PRM7 promoted phase separation of endophilin in the presence of PEG (**Figure 2E**) could also be considered as a lowering of the phase boundary of the endophilin/TIL or endophilin/PRM7 systems in the presence of PEG.

We asked, whether LLPS in the presence of TIL and PRM7 is predominantly driven via multivalent interactions with endophilin-SH3 domain or, alternatively, the phase separation is promoted by excluded volume effects caused by these disordered peptides. We determined the volume occupancies of TIL, PRM7, and PEG from their specific volumes (see *Methods*) at the threshold concentrations of those molecules required for driving LLPS at the common reference concentration for endophilin of 20 µM. The estimated volume occupancies of TIL and PRM7 at the corresponding threshold concentrations (20 µM and 10 µM respectively according to **Figure 3E, 3F**) were found to be about 300 times lower than that of PEG (at 5% w/v, see **Figure 1B**). This suggests that, at the concentrations of TIL and PRM7 that drives LLPS, the excluded volume effect would have minimal contributions. Multivalent interaction driven LLPS can have major functional implications in the formation of protein assembly during FEME.

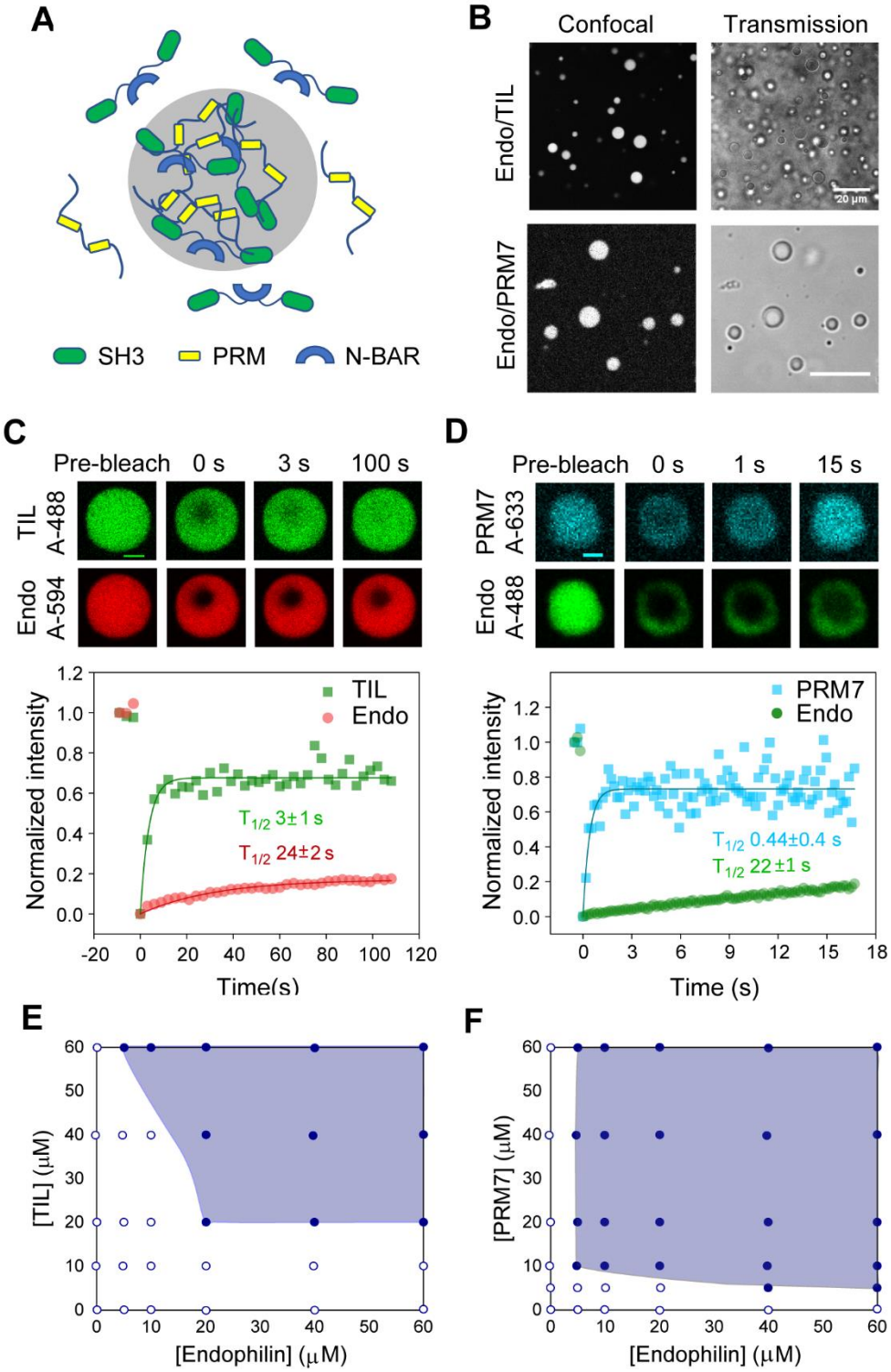

Figure 3: Endophilin undergoes LLPS through multivalent interactions with proline-rich-motifs. A. Cartoon diagram illustrating that multivalent interaction between SH3 domains of dimeric endophilin and a multiple PRM containing ligand can drive LLPS. **B.** Confocal fluorescence images (left) and transmission images (right) of droplets formed by the TIL/endophilin (top) and PRM7/endophilin (bottom) system. The droplets were doped with either TIL-Alexa 488 or PRM7-Alexa 633 for fluorescence imaging. Scale bar 20

μm. **C.** Images and intensity profiles from FRAP studies on a TIL/endophilin droplet to monitor the mobility of both endophilin (Alexa 594) and TIL (Alexa 488). Recovery time constants were determined from single-exponential fits (solid lines) of the FRAP data. TIL shows a faster recovery whereas endophilin shows a slower and partial recovery. **D.** FRAP study on PRM7/endophilin droplet in the presence of endophilin-Alexa 488 and PRM7-Alexa 633. PRM7 shows faster recovery than TIL whereas endophilin recovery was comparable to the TIL/endophilin system. **E, F**. Phase diagram for TIL/endophilin LLPS system (E) and the PRM7/endophilin LLPS system (F).

Endophilin causes clustering of membrane bound TIL and PRM7 by two-dimensional phase separation

Prior to receptor activation, endophilin is recruited by LPD at the leading edge of the cells and forms transient clusters that act as FEME priming sites (13). Followed by ligand activation, receptors are sorted into endophilin-rich clusters through TIL-SH3 interactions (**Figure 4A**). From our bulk experiments, it is evident that endophilin forms liquid-like droplets upon multivalent interactions with both LPD PRMs and TIL. We hypothesized that on the membrane such multivalent interactions play crucial role in the formation of endophilin-rich clusters with LPD as well as during sorting of receptors into the clusters. Earlier studies have shown that certain signaling proteins can undergo LLPS via multivalent interactions to form submicron sized clusters on the membrane (20,24). We first determined to what extent endophilin can cause clustering of TIL and LPD PRMs on the membrane. For this study, we prepared solid supported bilayers (SSBs) with tethered TIL-His_6 or PRM7-His_6 via Ni^{2+}-NTA lipids (**Figure 4B**). Both peptides were uniformly distributed and freely mobile on the bilayers (**Figure 4C** and *Supplementary Figure 9A*). To study the effect of endophilin on the bilayers, we utilized the ΔH0 mutant of endophilin instead of the full-length protein since the latter was shown to destroy supported lipid bilayers by insertion of its H0 helix (54). In bulk experiments, the ΔH0 mutant of endophilin showed similar phase behavior as the full length protein and also formed LLPS droplets in the presence of TIL (**Figure 1F** and *Supplementary figure 10*). Within 5 min of adding endophilin (ΔH0) we observed submicron sized clusters forming both in the case of TIL and PRM7 tethered bilayers. When imaged after 30 min, the clusters looked bigger and brighter and the intensity around the clusters depleted indicating active sequestration of proteins into the clusters from the surroundings (**Figure 4C**). Endophilin colocalized with both TIL and PRM7 in the clusters (**Figure 4D, 4E**). The extent of clustering was quantified by a radial average autocorrelation function (55) (**Figure 4F**).

Enhanced clustering (larger correlation length) was observed by increasing endophilin concentration from 1 μM to 2.5 μM (**Figure 4C, 4F)**. FRAP studies on the clusters showed partial photorecovery of both TIL and PRM7 indicating liquid-like properties of the clusters (*Supplementary figure 9B*). Altogether, these results provide strong evidences behind our hypothesis that clustering of endophilin in the presence of LPD at the FEME priming sites are driven by phase separation via multivalent interactions between endophilin SH3 and LPD PRMs. Moreover, the observation that interactions between endophilin and TIL leads to cluster formation on the membrane suggests TIL might have a catalytic role in the maturation of transient endophilin clusters to stable transport carriers.

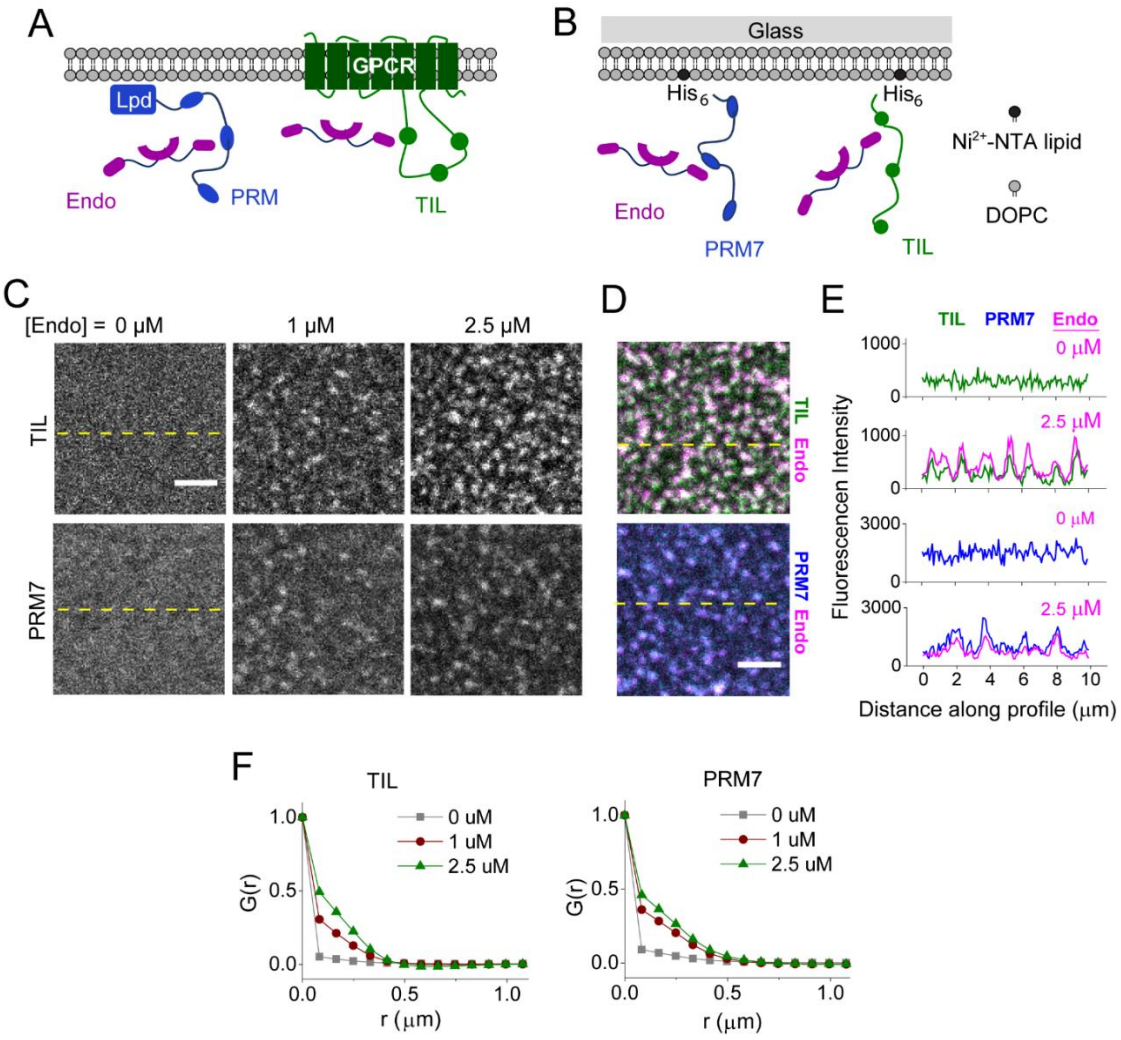

Figure 4: Endophilin causes clustering of both TIL and PRM7 on the membrane. A. Cartoon representation of the interactions between endophilin and proline-rich-motifs of GPCR-TIL and LPD C-terminal domain on cell membrane. **B**. An *in vitro* model system that has been developed to mimic the

endophilin-LPD-GPCR interactions using solid-supported bilayers (SSBs) with conjugated PRM7-His_6 and TIL-His_6 via Ni^{2+}-NTA-lipids (right). **C**. Confocal images showing distributions of TIL-Alexa 488 (top) and PRM7-Alexa 633 (bottom) on SSBs composed of Ni^{2+}-NTA lipid and DOPC (1:99). Images were recorded after incubating the functionalized SSBs with 0-2.5 µM endophilin for 35 min. Scale bar 2.5 µm. **D.** Merged images of endophilin-Alexa 594 channel with either TIL-Alexa 488 channel (top) or PRM7-Alexa 633 channel (bottom) in the presence of 2.5 µM endophilin. Scale bar 2.5 µm. **E.** Intensity profiles along the yellow lines shown in fig. 4B and fig. 4C showing that clustering of TIL and PRM7 occurred in the presence of endophilin and endophilin colocalized with TIL and PRM7 in the clusters. **F.** Radially averaged normalized autocorrelation function $G(r)$ demonstrating the degrees of clustering in the TIL (left) and PRM7 (right) channels at 0-2.5 µM of endophilin. The function $G(r)$ determines the probability of finding a fluorescent pixel at a given distance r from a center pixel.

<u>TIL initiates cluster formation in a pre-existing endophilin-PRM7 system on the membrane</u>

We have demonstrated that endophilin can drive cluster formation of membrane coupled TIL and PRM7 (**Figure 4**). Next, we asked with PRM7 and TIL co-existing on the membrane, whether endophilin induces co-clustering of TIL and PRM7 or if the cluster formation would be mutually exclusive. TIL showed a tendency to form clusters when introduced to the bilayer at an equimolar concentration (500 nM) along with PRM7 *(Supplementary Figure 11*). Self-clustering of TIL was minimized by reducing the concentration (50 nM) of TIL used for membrane-tethering (**Figure 5A**, top panel). We confirmed the fluidity of both TIL and PRM7 on the bilayers by FRAP *(Supplementary Figure 12)*. Within 1 min of incubation with endophilin (ΔH0), cluster formation was observed in fluorescence imaging channels corresponding to TIL, PRM7, and endophilin. Clusters appeared bigger in size and brighter when imaged 15 min after endophilin addition (**Figure 5A, 5B**). Interestingly, TIL showed a greater extent of clustering than PRM (**Figure 5A-C**). This indicates, when both TIL and PRM7 compete for cluster formation in the presence of endophilin, TIL exhibits a higher tendency to form clusters than PRM7. Cross-correlation analysis between TIL and PRM7 channels showed significant enhancement in the correlation function after addition of endophilin (**Figure 5D**). This data indicates that co-clustering of TIL and PRM7 was indeed promoted by endophilin and not due to the self-clustering of TIL and PRM7 that was observed at higher concentration of TIL. Co-clustering of TIL and PRM7 indicates both TIL and LPD PRMs act synergistically in the cluster formation during the formation of transport carriers during FEME. A comparatively higher

clustering tendency in TIL than PRM7 motivated us to investigate further if endophilin-TIL interactions can have triggering activity on a bilayer containing pre-enriched endophilin through LPD PRMs.

To test whether introduction of TIL can catalyze formation of protein assembly in the presence of endophilin and PRM7 pre-enriched on a bilayer, we first formed supported lipid bilayers containing tethered PRM7 and then recruited endophilin onto it. Introduction of endophilin caused clustering of PRM7 as expected (**Figure 5E, 5F**). Next, TIL (50 nM) was added to the system. Within 5 min, TIL started forming new clusters that were enriched in TIL, endophilin and PRM7. The clusters appeared bigger and brighter when imaged 15 min after adding TIL indicating accumulation of proteins from the membrane surroundings into the clusters (**Figure 5E, 5F**). Both PRM7 and endophilin colocalized with TIL in the clusters (**Figure 5F**). Autocorrelation analysis showed larger values of the autocorrelation function in the presence of TIL indicating that TIL causes significant enhancement in the clustering on a membrane pre-enriched with endophilin and PRM7 (**Figure 5G**). Cross-correlation analysis illustrated a stronger correlation between TIL-endophilin, PRM7-endophilin, and TIL-PRM7 channels after addition of TIL indicating that TIL induces co-partitioning of all three proteins into the clusters (**Figure 5H**). These results altogether imply that TIL can trigger PRM-endophilin-TIL co-assembly on the membrane via multivalent interactions. Interactions between receptor TIL with endophilin pre-enriched at the priming sites has been proposed as an essential step for the initiation of FEME (13,14). Here, we provide evidence that protein-protein phase separation driven by PRM-endophilin-TIL system plays key mechanistic roles in the formation of transport carriers in FEME.

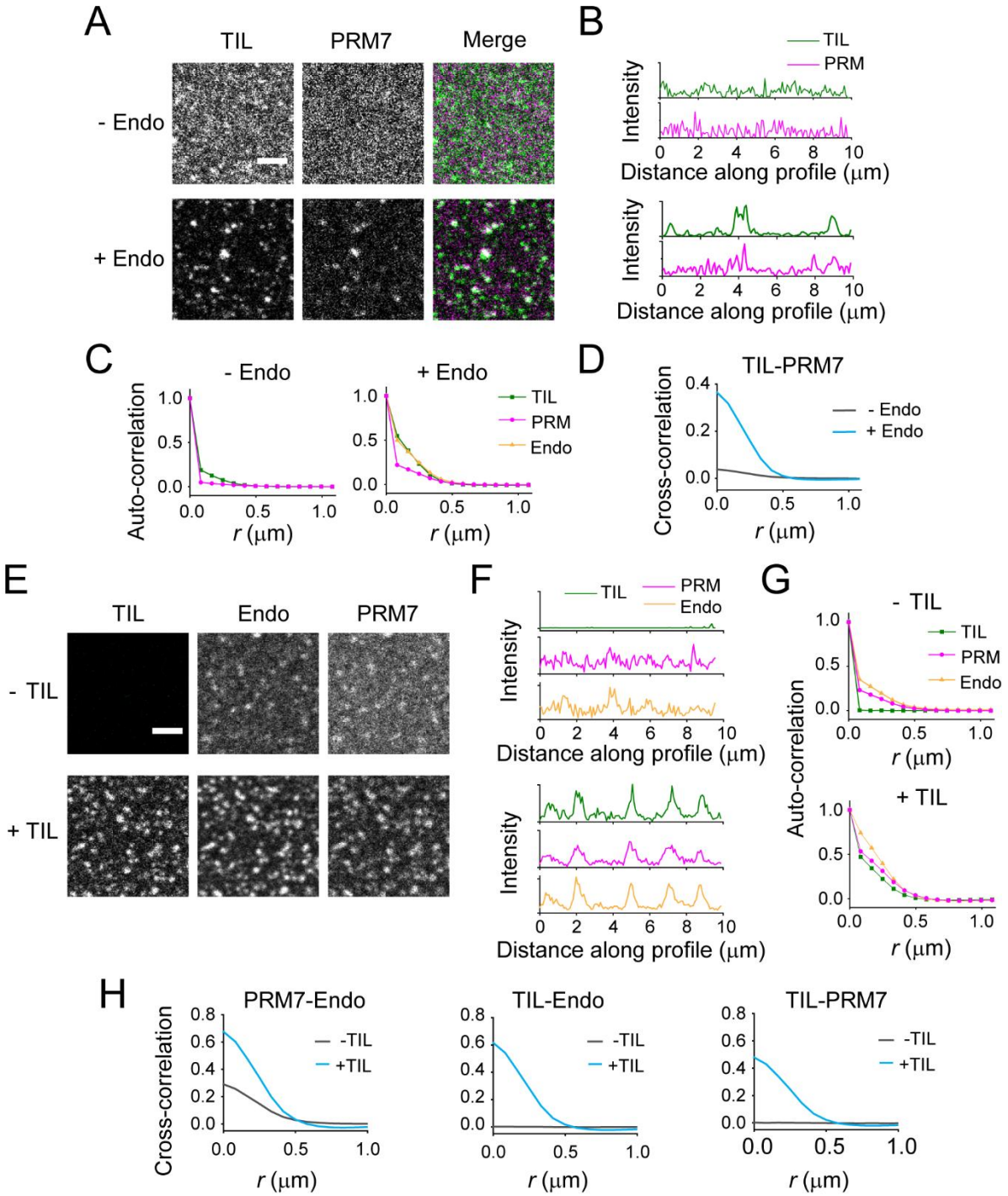

Figure 5: TIL exhibits stronger clustering abilities than PRM7 and triggers cluster formation in a membrane pre-enriched with endophilin. A. Confocal images of SSBs with conjugated His_6 tagged TIL (Alexa 488) and PRM7 (Alexa 633) in the presence and absence of endophilin (10% Alexa 594 labeled). Scale bar 2.5 µm. **B.** Fluorescence intensity profiles for the images shown in fig. 5A demonstrating the extent of co-localization of TIL and PRM7 within the clusters. **C.** Radially averaged, normalized autocorrelation functions demonstrating the clustering in the TIL, PRM7 and endophilin channels before (top) and after (bottom) addition of endophilin. **D.** Cross-correlation functions showing the extent of co-clustering between the TIL and PRM7 before and after addition of endophilin. **E.** Protein distribution on the

SSBs containing tethered PRM7 and endophilin before and after addition of TIL (50 nM). **F.** Fluorescence intensity profiles for the images shown in fig. 5D showing co-localization of TIL and PRM7 into the clusters. **G.** Extent of clustering in the TIL, PRM7 and endophilin channels before (top) and after (bottom) addition of TIL quantified by radially averaged autocorrelation function. **H.** Cross-correlation functions demonstrating co-clustering of the PRM7-endophilin, TIL-endophilin, and TIL-PRM7 system. The grey and the cyan curves denote the cross-correlation functions before and after the addition of TIL respectively.

Discussion

The importance of LLPS is evident from its association with an increasing number of biological phenomena ranging from formation of membraneless organelles to clustering of signaling proteins on the membrane (35,42). LLPS is facilitated by multivalent interactions that can be achieved through either self-association or binding with another multivalent ligand (19). Recently, LLPS has been considered to serve as a key mechanism of protein assembly formation in CME (56). Here we demonstrate that the BAR-protein endophilin that is associated with both CME and CIE undergoes LLPS via both N-domain driven self-association as well as through SH3 domain mediated multivalent interactions with its binding partners (**Figure 6**), both in the bulk, as well as on membranes. Our results suggest that LLPS could play crucial roles in formation of endophilin rich clusters on the plasma membrane, where the clusters serve as initiation sites for FEME. The liquid like clusters allow sorting of activated receptors that also act as multivalent binding partners of endophilin in a process that leads to formation of transport carriers (13).

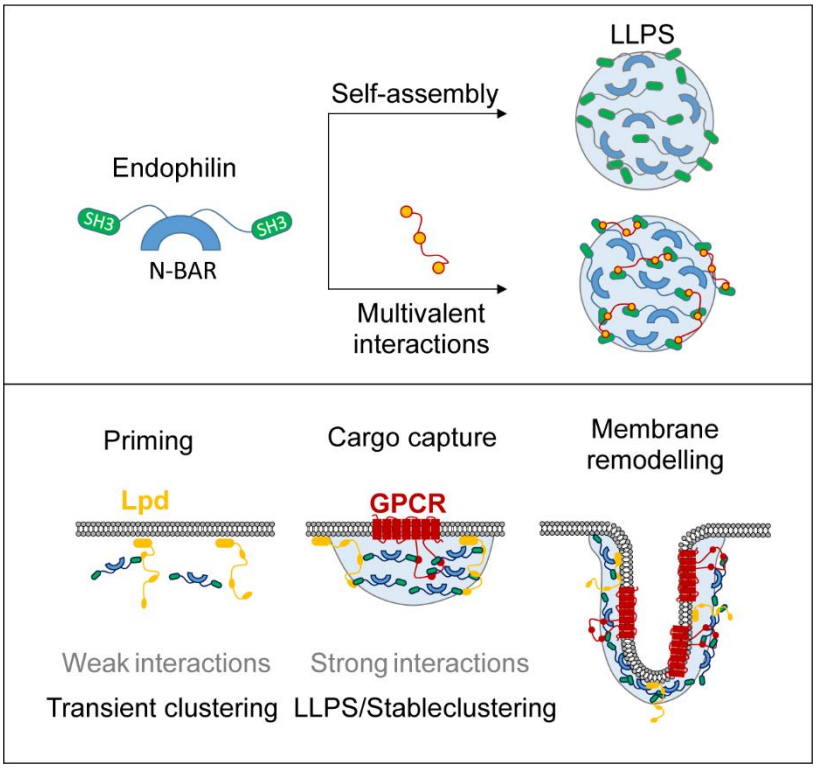

Figure 6: Working model for the role of phase separation in sequestration of endocytic proteins and membrane remodeling in FEME. Endophilin undergoes LLPS via both self-assembly of the BAR-domains and multivalent interactions with binding partners mediated by the SH3 domains. Depending on the strength of the binding interactions endophilin forms transient or stable clusters with other endocytic proteins. Weak interactions with LPD-PRM lead to formation of transient clusters prior to receptor activation. Receptor activation enables stronger interactions with TIL and facilitates stable cluster formation. Liquid-like clusters allow sequestering activated receptors and other binding partners of endophilin by partitioning. We propose that LLPS driven protein clustering on membrane facilitates membrane remodeling during CIE.

FEME is driven by rapid (within 10 sec) assembly and disassembly of more than 10 types of proteins within submicron sized membrane domains (13,15). In the biological system, protein assembly is often regulated by LLPS that forms a condensed phase via multivalent interactions between proteins and nucleic acids known as scaffolds (42). These-phase separated scaffolds can further concentrate client proteins on the basis of their abilities to partition in scaffolds. As we show here, inherent scaffold formation abilities can facilitate protein assembly in endocytic processes by allowing partitioning of its binding partners as clients. Similar to other LLPS systems, we found scaffold-client interactions to enhance or to suppress LLPS depending on the nature of their specific interactions with endophilin (43). Notably, promotion of LLPS by

two crucial multivalent clients – PRM7 of LPD and TIL of β1-AR suggests that these proteins might be engaged in a switch-like action in endocytosis to initiate protein condensation by shifting the phase boundary to lower endophilin concentration (**Figure 6**). It is likely that the liquid-like clusters further facilitate recruitment of downstream effector proteins such as dynamin that is known to be recruited by endophilin during FEME to promote membrane scission (15).

A key question is how membrane curvature generation in FEME is associated with receptor activation (13,15). When present on the membrane at sufficiently high density, endophilin alone can generate membrane tubules via its N-BAR domain (21,57). However, membrane invaginations are only observed after receptor activation. A current hypothesis suggests that receptor activation enables TIL-mediated recruitment of endophilin to the membrane that possibly enhances the local concentrations of endophilin beyond the threshold required to cause membrane deformation (13,14). We establish here that TIL triggers clustering of endophilin on the membrane via LLPS driven by multivalent interactions involving the SH3 domain of endophilin. Membrane remodeling can occur both through enhancement of local endophilin N-BAR activity within the clusters and promotion of membrane scaffolding by rigid N-BAR assembly. In a recent report, Bergeron-Sandoval *et al* has proposed that mechanical forces applied on the membrane by viscoelastic protein condensates formed in CME can facilitate membrane deformation (58). However, another recent study by Yuan *et al.* shows protein phase separation on the membrane surface creates a compressive stress on the lipid bilayer that causes membrane curvature but at an opposite direction to the curvatures generated by N-BAR proteins (59). In order to understand whether these mechanical effect would facilitate or inhibit the curvature generation by a phase separated N-BAR protein, careful experimental design with appropriate model membrane system will be needed to test these ideas. This work is currently ongoing.

Summary

In our contribution, we show that the phase separation of endophilin, combined with the driver plus regulator actions of multivalent binding partners of the endophilin-SH3 domain, results in the formation

and regulation of endocytic protein complexes. Liquid-like assembly of endocytic proteins could help accomplish two critical aspects of FEME – 1) dynamic formation of endophilin rich molecular scaffolds to serve as initial cargo capture sites, and 2) sorting of activated receptors and sequestration of various endocytic proteins via client-partitioning into the scaffolds. The multivalent binding partners, depending on their specific molecular interactions with endophilin on the membrane, can have different efficiencies to form clusters. Stronger cluster formation shown by the TIL over LPD-PRMs could result, after receptor activation, in a driving force for the maturation of transient clusters. These clusters, formed by endophilin-LPD complexes at the FEME initiation sites, would then lead to the formation of stable membrane transport carriers (13-15). Our findings further suggest that endophilin-TIL interactions enabled by receptor activation is a crucial step in the formation of endocytic protein complexes during FEME. An important question therefore arises: can endophilin binding to TIL trigger FEME in cells? Current efforts in the lab are directed toward understanding the implications of local activation of endophilin-TIL interactions in membrane trafficking. Formation of liquid-like assembly by multivalent protein-protein interactions might also drive steps downstream of cargo sorting such as engagement of actin regulatory machinery involving N-WASP and Arp2/3 (15) and membrane scission via endophilin-dynamin complexes (60). Here we provide evidence suggesting that phase separation behavior of endocytic proteins driven by endophilin self-association as well as multivalent interactions involving both adaptors and receptors could be the mechanistic handle in understanding the formation and regulation of protein assembly in clathrin-independent membrane trafficking.

Materials

Chemicals. Alexa Fluor™-488 C5-maleimide, Alexa Fluor™-488 5-SDP ester, Alexa Fluor™-594 C5-maleimide, Alexa Fluor™-633 C5-maleimide, and Alexa Fluor™-647 conjugated bovine serum albumin were procured from ThermoFisher Scientific (USA). Alexa Fluor™-488-αSynuclein was generously provided by Elizabeth Rhoades' lab. Polyethylene glycol (average MW 8,000) was obtained from Sigma-Aldrich (USA). Tris(2-carboxyethyl)phosphine hydrochloride (TCEP-HCl) was obtained from AlfaAesar (USA). Sucrose and common reagents for buffer preparation including HEPES, Tris, NaCl, Na_2HPO_4 and NaH_2PO_4, dithiothreitol (DTT), and ethylenediaminetetraacetic acid

(EDTA) were obtained from Fisher Scientific (USA). Lipids 1,2-dioleoyl-sn-glycero-3-phosphocholine (DOPC) and 1,2-dioleoyl-sn-glycero-3-[(N-(5-amino-1-carboxypentyl)iminodiacetic acid)succinyl] (nickel salt) (Ni-NTA DOGS) were purchased from Avanti Polar lipids (AL, USA).

Plasmids. Full-length rat endophilin A1 [mutated to a single-cysteine form for labeling, C108S, E241C, C294,295S], endophilin-N-BAR, and endophilin-dH0 were encoded by plasmids described previously (61). Plasmids encoding human amphiphysin 1, as well as a truncate in the form of the N-BAR domain were provided by Pietro De Camilli's lab. FBP17 was obtained from Harvey McMahon's lab. The pMal-Abl-PRM5R plasmid was a generous gift from Michael Rosen's Lab (Addgene plasmid #112088). The sequence encoding 7x repeats of a PRM from lamellipodin (aa 970-981) containing $(Gly\text{-}Gly\text{-}Ser)_4$ linkers was custom synthesized by Biomatik Corporation (Canada). The PRM7 sequence was cloned into the pMal-Abl-PRM5R plasmid by replacing its PRM5 sequence. The C-terminal TEV protease cleavable site between the PRM7 and the 6x His tag was further mutated to stop the cleavage of the His tag during purification. TIL of human β-1 adrenergic receptor was cloned into a pGEX6p1 vector as described elsewhere (11); a TIL sequence with a polyhistidine tag was synthesized and inserted into pGEX6p1 vector by Biomatik Corporation (Canada). See Supporting Information for sequence information.

Methods

Protein Expression and Purification

BL21-CodonPlus(DE3)-RIL cells (Agilent Technologies) were transformed with the plasmid of interest. Large volume cultures (2x 1 L for TIL and TIL-His, 4x 1 L for PRM7-His, amphiphysin N-BAR, FBP17, endophilin, endophilin dH0 and N-BAR; 8 L for amphiphysin) were grown from starter culture (100 mL), shaking at 225 RPM at 37 °C until O.D. at 600 nm reached 0.5-0.8. Cultures were induced with IPTG (300 µM for TIL and TIL-His, 600 µM for amphiphysin, amphiphysin-N-BAR, endophilin, endophilin ΔH0, and N-BAR, 1 mM for FBP17 and PRM7-His) and expression was carried out at 18 °C for ~16 h. Cells were harvested by centrifugation at 6000 rpm for 10 min, resuspended in a lysis buffer (300 mM NaCl, 50 mM Tris, 2 mM DTT, 1 mM EDTA, pH 8.0) containing 1 mM PMSF. The lysis buffer contained additional 20 mM imidazole but no EDTA for PRM7-His. For amphiphysin N-BAR, 10% glycerol was added to the lysis buffer. Bacterial cells were lysed by tip sonication, and centrifuged at 16,000 rpm for

1 h to remove debris. The supernatant was filtered through 0.22 µm-pore syringe-tip filters (Millipore-Sigma), then purified by FPLC. Protein specific details of the purification methods are given below.

TIL and TIL-His. Both TIL and TIL-His were purified following a methodology described elsewhere (11). Cell lysate was prepared as described above. In short, the GST tagged protein was purified from the cell lysate by GST Trap affinity chromatography (GE Healthcare). The GST tag was cleaved from TIL by PreScission protease, and the resulting protein mixture was purified by a gradient elution of a HiTrap SP HP cation exchange column (GE Healthcare).

Purification LPD C4 PRM7-His. The PRM7-His construct was expressed as an N-terminal MBP and C-terminal His-tagged fusion. Cell lysate was prepared as described above and loaded to a HisTrap HP affinity column (GE Healthcare) with the help of the EDTA-free lysis buffer containing imidazole as described above. Bound protein was washed with the lysis buffer and eluted with a high-imidazole elution buffer (300 mM NaCl, 50 mM Tris, 2 mM DTT, 500 mM imidazole, pH 8.0). The elution was loaded to a HiTrap SP HP cation exchange column (GE Healthcare) and eluted over a gradient of NaCl (150 mM NaCl, 20 mM sodium phosphates (monobasic and dibasic), pH 7.0, 1 mM EDTA, 1 mM TCEP; buffer B: 1 M NaCl, 20 mM sodium phosphates (monobasic and dibasic), pH 7.0, 1 mM EDTA, 1 mM TCEP). Fractions containing PRM construct were identified via SDS-PAGE.

PRM7-His fractions were dialyzed against 2 x 1 L of anion exchange buffer A (150 mM NaCl, 50 mM Tris, 1 mM EDTA, 1 mM DTT, pH 8.0) using a dialysis membrane having 3500 kDa molecular weight cut-off (Fisherbrand) for 12 h, at 4 °C. The dialyzed protein was loaded onto an anion exchange Q HP column (GE Healthcare) and MBP-PRM7-His was collected as flow through. The flow through was cleaved with TEV protease [~1 mg in 15 mL] at 4 °C for ~12 h. Following cleavage, the protein mixture was passed over amylose resin (New England BioLabs). Pure PRM7-His was collected as flow through, concentrated in Amicon™Ultra centrifugal filters (Millipore-Sigma) and exchanged with a HEPES buffer (20 mM HEPES, 150 mM NaCl, 1 mM TCEP, pH 7.4). Concentrations were determined from the tryptophan absorption at 280 nm (ε_{280} 5500 $M^{-1}cm^{-1}$) using a Nanodrop instrument (Thermo Scientific).

Purification of Endophilin, Endophilin-N-BAR, Endophilin-dH0, Amphiphysin, Amphiphysin N-BAR,

Full length endophilin A1, endophilin ΔH0, and the N-BAR-only mutant were expressed as GST fusion proteins and purified as described previously (11,40). Briefly, the cell lysate obtained as described above was put through GST-affinity chromatography. After elution was collected, GST tags were cleaved using PreScission protease. Cleaved

proteins were further purified by anion exchange chromatography followed by size exclusion chromatography. SDS-PAGE was conducted between chromatography steps to determine protein purity. Final protein concentrations were determined by absorption at 280 nm (via Nanodrop). Purification of amphiphysin and its N-BAR domain was performed following the same protocol as described for endophilin with the following modifications. Both proteins were purified by cation exchange chromatography after the protease cleavage. Additionally, for amphiphysin-N-BAR all buffers used for the purification contained 10% glycerol.

Purification of FBP17

Cell lysate was prepared as described above and loaded to a GSTrap™FF column (GE Healthcare) in lysis buffer (300 mM NaCl, 50 mM Tris, 2 mM DTT, 1 mM EDTA, pH 8.0). The column was washed with a wash buffer (150 mM NaCl, 50 mM Tris, 2 mM DTT, 1 mM EDTA, pH 8.0) and the protein was eluted with a glutathione-containing buffer (150 mM NaCl, 50 mM Tris, 2 mM DTT, 1 mM EDTA, 20 mM glutathione, pH 8.0). Eluted protein was simultaneously digested with PreScission protease and dialyzed across a membrane (Fisherbrand) into a glutathione-free buffer (150 mM NaCl, 50 mM Tris, 1 mM EDTA, 1 mM DTT, pH 8.0). Dialyzed and cleaved protein was finally purified by size exclusion chromatography in a HEPES buffer (150 mM NaCl, 20 mM HEPES, 1 mM TCEP, pH 7.4).

Fluorescent Labeling

TIL and TIL-His were labeled at the N-terminal with Alexa Fluor™-488 5-SDP ester; protein was exchanged to an amine-free buffer (20 mM sodium phosphates, 150 mM NaCl, pH 7.0) and label was added to the protein in 5 times molar excess and allowed to react for 24-36 h at 4 °C. FBP17, amphiphysin, PRM7-His, endophilin, and endophilin truncations were labeled with a 5C-maleimide-linked fluorophores, with label added to the protein at a 5 times molar excess and allowed to react for either 4h (FBP17) or 12-16h (PRM7-His, amphiphysin, endophilin and its mutants). In all cases, labeled protein was separated from excess dye by passing over HiTrap™ desalting columns (2x5 mL) (Cytiva).

Protein Concentration Determination after Labeling

For endophilin and its mutants, amphiphysin, FBP17, and PRM7-His, the protein absorbance at 280 nm and the fluorescent label absorbance at the corresponding wavelengths were measured using a Nanodrop instrument. The contributions from the fluorophore to the absorption at 280 nm were determined from the absorption spectra of protein free fluorophores and were subtracted from the absorbance of the labeled protein to determine the protein concentration accurately.

TIL and TIL-His concentrations could not be determined from absorption at 280 nm since they have no tryptophan. First, the concentration of fluorescently labeled protein was determined from the fluorophore absorbance using a Nanodrop instrument. In order to obtain the total protein concentration, the mixture of labeled and unlabeled proteins was injected onto a ZORBAX Eclipse XDB C8 HPLC column (Agilent, USA) and eluted with a gradient of acetonitrile and water (Solvent A: water and 0.1% trifluoroacetic acid, Solvent B: acetonitrile with 0.1% trifluoroacetic acid) using an LC-10AT solvent delivery systems (Shimadzu Corporation). Chromatograms at 220 nm (peptide) and 340 nm (for the secondary absorption band of Alexa 488) were recorded via SPD-10A detector (Shimadzu Corporation). The labeled and the unlabeled proteins appeared as two different peaks in the chromatogram. The relative concentrations of the labeled and unlabeled proteins were determined from the ratio of the area under the two peaks. Concentration of the unlabeled protein was estimated from the ratio and the concentrations of the labeled protein obtained via Nanodrop measurements.

Construction of Phase Diagrams

Phase diagrams were built by scoring protein mixtures at the given protein and PEG concentrations for the presence of droplets with transmitted light microscopy. For these experiments, protein solutions (10 µL) in HEPES buffer were visualized in a 384-well plate (Greiner Bio-One, Austria) with an Olympus IX71 inverted microscope using a 40x 0.75 NA air objective (Olympus, Center Valley, PA).

Confocal Microscopy

Confocal imaging was performed using an Olympus IX83 inverted microscope equipped with FluoView 3000 scanning system (Olympus, Center Valley, PA). Images were taken at room temperature using a 60x 1.2 NA water immersion objective (Olympus). Imaging of multi-protein systems was performed via orthogonal fluorescent labelling of proteins using Alexa 488 (λ_{ex} 488 nm, λ_{em} 500–540 nm), Alexa 594 (λ_{ex} 561 nm, λ_{em} 580–620 nm), and Alexa 633 (λ_{ex} 640 nm, , λ_{em} 650–700 nm). The excitation lasers were alternatively used to minimize cross-talk between the different channels. Images were analyzed with ImageJ, MATLAB, and Python programs.

For imaging droplets in solution, glass coverslips (25 × 25 mm^2, Fisher Scientific) passivated with BSA (2 mg/mL in HEPES buffer) were used. Solutions (5-10 µL) containing the droplets were imaged in a closed chamber created by sandwiching two coverslips (25 × 25 mm^2, Fisher Scientific) using vacuum grease. For supported bilayers, a chamber formed from coverslips (see Planar Supported Bilayer Preparation section) were used for imaging.

Fluorescence Recovery after Photobleaching (FRAP) studies on droplets

For FRAP studies, a circular region of interest (ROI) within a protein condensate settled on the glass coverslip was bleached using short exposures (~ 500 ms) of either 488 nm or 561 nm or 640 nm lasers at 100% laser power. The ROI size and the bleach time were adjusted to keep the bleach area <= 20% of the droplet area. Collection of images for the recovery stage was started immediately after the bleaching. FRAP data were analyzed using ImageJ (for image intensity extraction) and Microsoft Excel (for quantitative analysis). For each time frame, mean intensities were estimated for an ROI within the bleached region and of another ROI from the unbleached region. The ratio of intensities at bleached ($I_{\text{bleach}}(t)$) and unbleached regions ($I_{\text{unbleach}}(t)$) were determined at each time point which was further normalized to 1 for the intensity ratio before photobleaching ($q(t_{\text{prebleach}})$) and to 0 for the intensity ratio at 0 s after photobleaching ($q(t_0)$) using the following formula:

$$I_{norm}(t) = \frac{q(t) - q(t_0)}{q(t_{prebleach}) - q(t_0)}$$

where $q(t) = \frac{I_{bleach}(t)}{I_{unbleach}(t)}$

The normalized intensities were plotted against time to obtain a fluorescence recovery profile. The recovery profile was fit to either a single exponential model,

$$I(t) = A(1 - e^{-\frac{t}{\tau}})$$

or a or double-exponential model, $I(t) = A\{B(1 - e^{-\frac{t}{\tau_1}}) + (1 - B)(1 - e^{-\frac{t}{\tau_2}})\}$,

as described elsewhere (37). A represents the mobile fraction and B represents fractional contribution of the time component τ_1. The values of A and B were limited to the interval [0,1] and time constants $(\tau, \tau_1, or\ \tau_2)$ were limited to the interval $[t_{frame}, \infty]$ where t_{frame} is the spacing between frames in a given FRAP experiment.

Apparent Partition Coefficients

Partition coefficients were determined following an earlier reported method (42). A typical experiment consisted of preparing a 10 µL suspension of endophilin (25 µM) droplets in the presence of 10% PEG. The partitioning proteins (clients) labeled with an Alexa™ fluorophore were mixed with endophilin, at a concentration between 250 nM-1 µM, prior to introducing the droplet formation by adding PEG. Droplet samples for confocal imaging were prepared as described above. The photodetector settings were optimized to ensure both bulk and droplet fluorescence intensities were above background but below the saturation level of the detector. Images were collected at the equatorial plane of the droplet and 10 and 20 droplets were imaged per experiment. Fluorescence intensities at the interior of droplets and in the bulk solution surrounding them were obtained using ImageJ. The background intensity was estimated by

imaging a solution containing no fluorescent protein under identical imaging conditions. The apparent partition coefficient is defined as the ratio of the background subtracted intensities inside and outside the droplet.

Droplet size determination from confocal images

Droplet size was determined from the confocal images using ImageJ. First, a binary image was created from an experimental image by applying Bandpass filter FFT method followed by threshold adjustment. Next, areas of all individual circular objects in the images were determined separately using the Analyze Particle tool. From the area, the diameter of each particle was determined.

Determination of volume occupancies of PEG, TIL and PRM7

Volume occupancy (φ) was defined as, $\varphi = c\ v$ where, c is concentration of the component and v is its specific volume (31). For PEG, the literature reported value of v, 0.84 ml/g was used (31). For, TIL and PRM7, v was estimated from their hydrodynamic radii (R) using the formula (62),

$$v = \frac{4\pi R^3 N_A}{3M}$$

where, N_A is the Avogadro's number and M is the molecular weight. We estimated the R values for TIL and PRM7 from their sequences using a formula established by Marsh and Forman-Kay (63).

Planar Supported Bilayer Preparation

Liposomes were prepared following a method described elsewhere (64), with minor modifications. Briefly, a lipid mixture containing DOPC and Ni^{2+}-NTA-DOGS (99:1) was dried under a stream of nitrogen, and vacuum dried for a time period between 2 and 16 hours. The lipid film was rehydrated in HEPES buffer with a final concentration of 1 mg/mL, by vortexing for 1 min in 10 sec intervals. The solution was sonicated for 30-40 min at room temperature, and subsequently subjected to five rapid freeze-thaw cycles. Finally, the LUV suspension was extruded 15 times through a polycarbonate membrane of pore size 100 nm pore size.

Supported bilayers were prepared following a method described elsewhere (24), with minor modifications. Briefly, chambered glass coverslips (Lab-tek, Cat #155409) were cleaned by rinsing with 50 % (v/v) isopropanol, followed by an incubation in 10 M NaOH for 2 hours, and finally washed thoroughly with Milli-Q water. A freshly prepared LUV suspension was added to the coverslips and incubated for 30 min (150 µL, 0.5-0.7 mg/mL). The wells were washed with HEPES buffer (3 x 450 µL) to remove intact, unadsorbed liposomes. The wells were incubated with equal volume BSA (fatty acid free) solution (2 mg/mL, in HEPES buffer) for 30 min, and washed with HEPES buffer (3 x 450 µL). The bilayers were immediately used for protein conjugation.

Protein conjugation to planar supported bilayer

For single protein coupled bilayers, either PRM7 or TIL with His_6-tag (500 nM) was added to the solution and gently mixed. The protein was incubated for 15 min and was gently rinsed with HEPES buffer (2 x 600 µL). After protein conjugation, the bilayers were allowed to rest for 30 min for equilibration before subsequent experiments.

Two protein coupled bilayers were achieved by sequential coupling of PRM7 followed by TIL. Simultaneous addition of equimolar (250 nM) PRM7 and TIL resulted in starkly varied coupling of the two proteins, perhaps due to differences in the kinetics of the association. Therefore, PRM7 (250 nM) was first coupled to the bilayer as described above and allowed to rest for 15 min. TIL (50 nM) was then introduced to the solution and gently mixed. After 5-10 min of incubation, the solution was gently rinsed with HEPES Buffer (2 x 600 µL) and the bilayer was allowed to rest for 15 min. This method ensured substantial and uniform binding of both proteins on the bilayer. Higher protein concentrations and longer incubation periods led to the formation of protein clusters on the bilayers.

FRAP was performed on the bilayers to confirm the fluidity of the protein(s) and the bilayer. All experiments were performed within 4 hours of depositing LUVs on the coverslips.

Autocorrelation Analysis

Heterogeneity on bilayers were assessed using the normxcorr2 function in MATLAB. The function was used to obtain both autocorrelation and cross correlation of and between the various fluorescent channels, respectively. Radial averaging of the data was performed using a home build analysis method based on Python. The correlation data were fit using a single exponential function of the form $y(\mathrm{r}) = A + B*\exp(-r/D)$, where A,B,D are fit parameters and r is the distance in microns ($r > 0$). The parameter D is the correlation length.

References

1. Ferguson, S. S. (2001) Evolving concepts in G protein-coupled receptor endocytosis: the role in receptor desensitization and signaling. *Pharmacological reviews* **53**, 1-24
2. Irannejad, R., and von Zastrow, M. (2014) GPCR signaling along the endocytic pathway. *Current opinion in cell biology* **27**, 109-116
3. Sorkin, A., and Von Zastrow, M. (2002) Signal transduction and endocytosis: close encounters of many kinds. *Nature reviews. Molecular cell biology* **3**, 600-614
4. Vieira, A. V., Lamaze, C., and Schmid, S. L. (1996) Control of EGF receptor signaling by clathrin-mediated endocytosis. *Science* **274**, 2086-2089
5. Conner, S. D., and Schmid, S. L. (2003) Regulated portals of entry into the cell. *Nature* **422**, 37-44
6. Kaksonen, M., and Roux, A. (2018) Mechanisms of clathrin-mediated endocytosis. *Nature reviews. Molecular cell biology* **19**, 313-326
7. McMahon, H. T., and Boucrot, E. (2011) Molecular mechanism and physiological functions of clathrin-mediated endocytosis. *Nature reviews. Molecular cell biology* **12**, 517-533
8. Carman, P. J., and Dominguez, R. (2018) BAR domain proteins—a linkage between cellular membranes, signaling pathways, and the actin cytoskeleton. *Biophysical reviews* **10**, 1587-1604
9. Lo, W. T., Vujicic Zagar, A., Gerth, F., Lehmann, M., Puchkov, D., Krylova, O., Freund, C., Scapozza, L., Vadas, O., and Haucke, V. (2017) A Coincidence Detection Mechanism Controls PX-BAR Domain-Mediated Endocytic Membrane Remodeling via an Allosteric Structural Switch. *Developmental cell* **43**, 522-529 e524
10. Moravcevic, K., Oxley, C. L., and Lemmon, M. A. (2012) Conditional peripheral membrane proteins: facing up to limited specificity. *Structure* **20**, 15-27
11. Mondal, S., Narayan, K. B., Powers, I., Botterbusch, S., and Baumgart, T. (2021) Endophilin recruitment drives membrane curvature generation through coincidence detection of GPCR loop interactions and negative lipid charge. *Journal of Biological Chemistry* **296**
12. Mayor, S., Parton, R. G., and Donaldson, J. G. (2014) Clathrin-Independent Pathways of Endocytosis. *Cold Spring Harbor Perspectives in Biology* **6**
13. Ferreira, A. P. A., and Boucrot, E. (2018) Mechanisms of Carrier Formation during Clathrin-Independent Endocytosis. *Trends in cell biology* **28**, 188-200
14. Boucrot, E., Ferreira, A. P., Almeida-Souza, L., Debard, S., Vallis, Y., Howard, G., Bertot, L., Sauvonnet, N., and McMahon, H. T. (2015) Endophilin marks and controls a clathrin-independent endocytic pathway. *Nature* **517**, 460-465
15. Casamento, A., and Boucrot, E. (2020) Molecular mechanism of Fast Endophilin-Mediated Endocytosis. *Biochemical Journal* **477**, 2327-2345
16. Vehlow, A., Soong, D., Vizcay-Barrena, G., Bodo, C., Law, A. L., Perera, U., and Krause, M. (2013) Endophilin, Lamellipodin, and Mena cooperate to regulate F-actin-dependent EGF-receptor endocytosis. *Embo Journal* **32**, 2722-2734
17. Tang, Y., Hu, L. A., Miller, W. E., Ringstad, N., Hall, R. A., Pitcher, J. A., DeCamilli, P., and Lefkowitz, R. J. (1999) Identification of the endophilins (SH3p4/p8/p13) as novel binding partners for the beta1-adrenergic receptor. *Proceedings of the National Academy of Sciences of the United States of America* **96**, 12559-12564
18. Case, L. B., Zhang, X., Ditlev, J. A., and Rosen, M. K. (2019) Stoichiometry controls activity of phase-separated clusters of actin signaling proteins. *Science* **363**, 1093-1097
19. Li, P. L., Banjade, S., Cheng, H. C., Kim, S., Chen, B., Guo, L., Llaguno, M., Hollingsworth, J. V., King, D. S., Banani, S. F., Russo, P. S., Jiang, Q. X., Nixon, B. T., and Rosen, M. K. (2012) Phase transitions in the assembly of multivalent signalling proteins. *Nature* **483**, 336-U129

20. Su, X. L., Ditlev, J. A., Hui, E. F., Xing, W. M., Banjade, S., Okrut, J., King, D. S., Taunton, J., Rosen, M. K., and Vale, R. D. (2016) Phase separation of signaling molecules promotes T cell receptor signal transduction. *Science* **352**, 595-599
21. Mim, C., Cui, H., Gawronski-Salerno, J. A., Frost, A., Lyman, E., Voth, G. A., and Unger, V. M. (2012) Structural basis of membrane bending by the N-BAR protein endophilin. *Cell* **149**, 137-145
22. Simunovic, M., Evergren, E., Golushko, I., Prevost, C., Renard, H. F., Johannes, L., McMahon, H. T., Lorman, V., Voth, G. A., and Bassereau, P. (2016) How curvature-generating proteins build scaffolds on membrane nanotubes. *Proceedings of the National Academy of Sciences of the United States of America* **113**, 11226-11231
23. Shin, Y., and Brangwynne, C. P. (2017) Liquid phase condensation in cell physiology and disease. *Science* **357**
24. Banjade, S., and Rosen, M. K. (2014) Phase Transitions of Multivalent Proteins Can Promote Clustering of Membrane Receptors. *Elife* **3**
25. Huang, W. Y. C., Alvarez, S., Kondo, Y., Lee, Y. K., Chung, J. K., Lam, H. Y. M., Biswas, K. H., Kuriyan, J., and Groves, J. T. (2019) A molecular assembly phase transition and kinetic proofreading modulate Ras activation by SOS. *Science* **363**, 1098-1103
26. Case, L. B., Ditlev, J. A., and Rosen, M. K. (2019) Regulation of Transmembrane Signaling by Phase Separation. in *Annual Review of Biophysics, Vol 48* (Dill, K. A. ed.). pp 465-494
27. Hardenberg, M., Horvath, A., Ambrus, V., Fuxreiter, M., and Vendruscolo, M. (2020) Widespread occurrence of the droplet state of proteins in the human proteome. *Proceedings of the National Academy of Sciences of the United States of America* **117**, 33254-33262
28. McDonald, N. A., Vander Kooi, C. W., Ohi, M. D., and Gould, K. L. (2015) Oligomerization but not membrane bending underlies the function of certain F-BAR proteins in cell motility and cytokinesis. *Developmental cell* **35**, 725-736
29. Mim, C., Cui, H. S., Gawronski-Salerno, J. A., Frost, A., Lyman, E., Voth, G. A., and Unger, V. M. (2012) Structural Basis of Membrane Bending by the N-BAR Protein Endophilin. *Cell* **149**, 137-145
30. Simunovic, M., Evergren, E., Golushko, I., Prevost, C., Renard, H. F., Johannes, L., McMahon, H. T., Lorman, V., Voth, G. A., and Bassereau, P. (2016) How curvature-generating proteins build scaffolds on membrane nanotubes. *Proceedings of the National Academy of Sciences of the United States of America* **113**, 11226-11231
31. Annunziata, O., Asherie, N., Lomakin, A., Pande, J., Ogun, O., and Benedek, G. B. (2002) Effect of polyethylene glycol on the liquid-liquid phase transition in aqueous protein solutions. *Proceedings of the National Academy of Sciences of the United States of America* **99**, 14165-14170
32. Patel, A., Lee, H. O., Jawerth, L., Maharana, S., Jahnel, M., Hein, M. Y., Stoynov, S., Mahamid, J., Saha, S., Franzmann, T. M., Pozniakovski, A., Poser, I., Maghelli, N., Royer, L. A., Weigert, M., Myers, E. W., Grill, S., Drechsel, D., Hyman, A. A., and Alberti, S. (2015) A Liquid-to-Solid Phase Transition of the ALS Protein FUS Accelerated by Disease Mutation. *Cell* **162**, 1066-1077
33. Ray, S., Singh, N., Kumar, R., Patel, K., Pandey, S., Datta, D., Mahato, J., Panigrahi, R., Navalkar, A., Mehra, S., Gadhe, L., Chatterjee, D., Sawner, A. S., Maiti, S., Bhatia, S., Gerez, J. A., Chowdhury, A., Kumar, A., Padinhateeri, R., Riek, R., Krishnamoorthy, G., and Maji, S. K. (2020) alpha-Synuclein aggregation nucleates through liquid-liquid phase separation. *Nature Chemistry* **12**
34. Zhou, H.-X., Rivas, G., and Minton, A. P. (2008) Macromolecular crowding and confinement: biochemical, biophysical, and potential physiological consequences. *Annu. Rev. Biophys.* **37**, 375-397
35. Alberti, S., Gladfelter, A., and Mittag, T. (2019) Considerations and Challenges in Studying Liquid-Liquid Phase Separation and Biomolecular Condensates. *Cell* **176**, 419-434
36. Rogers, B. A., Rembert, K. B., Poyton, M. F., Okur, H. I., Kale, A. R., Yang, T. L., Zhang, J. F., and Cremer, P. S. (2019) A stepwise mechanism for aqueous two-phase system formation in

concentrated antibody solutions. *Proceedings of the National Academy of Sciences of the United States of America* **116**, 15784-15791

37. Kaur, T., Alshareedah, I., Wang, W., Ngo, J., Moosa, M. M., and Banerjee, P. R. (2019) Molecular Crowding Tunes Material States of Ribonucleoprotein Condensates. *Biomolecules* **9**
38. Taylor, N. O., Wei, M. T., Stone, H. A., and Brangwynne, C. P. (2019) Quantifying Dynamics in Phase-Separated Condensates Using Fluorescence Recovery after Photobleaching. *Biophysical Journal* **117**, 1285-1300
39. Wegmann, S., Eftekharzadeh, B., Tepper, K., Zoltowska, K. M., Bennett, R. E., Dujardin, S., Laskowski, P. R., MacKenzie, D., Kamath, T., Commins, C., Vanderburg, C., Roe, A. D., Fan, Z. Y., Molliex, A. M., Hernandez-Vega, A., Muller, D., Hyman, A. A., Mandelkow, E., Taylor, J. P., and Hyman, B. T. (2018) Tau protein liquid-liquid phase separation can initiate tau aggregation. *Embo Journal* **37**
40. Capraro, B. R., Shi, Z., Wu, T., Chen, Z., Dunn, J. M., Rhoades, E., and Baumgart, T. (2013) Kinetics of endophilin N-BAR domain dimerization and membrane interactions. *The Journal of biological chemistry* **288**, 12533-12543
41. Gallop, J. L., Jao, C. C., Kent, H. M., Butler, P. J., Evans, P. R., Langen, R., and McMahon, H. T. (2006) Mechanism of endophilin N-BAR domain-mediated membrane curvature. *The EMBO journal* **25**, 2898-2910
42. Banani, S. F., Rice, A. M., Peeples, W. B., Lin, Y., Jain, S., Parker, R., and Rosen, M. K. (2016) Compositional Control of Phase-Separated Cellular Bodies. *Cell* **166**, 651-663
43. Ghosh, A., Mazarakos, K., and Zhou, H. X. (2019) Three archetypical classes of macromolecular regulators of protein liquid-liquid phase separation. *Proceedings of the National Academy of Sciences of the United States of America* **116**, 19474-19483
44. Ringstad, N., Nemoto, Y., and De Camilli, P. (2001) Differential expression of endophilin 1 and 2 dimers at central nervous system synapses. *The Journal of biological chemistry* **276**, 40424-40430
45. Micheva, K. D., Ramjaun, A. R., Kay, B. K., and McPherson, P. S. (1997) SH3 domain-dependent interactions of endophilin with amphiphysin. *Febs Letters* **414**, 308-312
46. Murakami, N., Xie, W., Lu, R. C., Chen-Hwang, M. C., Wieraszko, A., and Hwang, Y. W. (2006) Phosphorylation of amphiphysin I by minibrain kinase/dual-specificity tyrosine phosphorylation-regulated kinase, a kinase implicated in Down syndrome. *Journal of Biological Chemistry* **281**, 23712-23724
47. Chan Wah Hak, L., Khan, S., Di Meglio, I., Law, A. L., Lucken-Ardjomande Hasler, S., Quintaneiro, L. M., Ferreira, A. P. A., Krause, M., McMahon, H. T., and Boucrot, E. (2018) FBP17 and CIP4 recruit SHIP2 and lamellipodin to prime the plasma membrane for fast endophilin-mediated endocytosis. *Nat Cell Biol* **20**, 1023-1031
48. Wu, M., Huang, B., Graham, M., Raimondi, A., Heuser, J. E., Zhuang, X. W., and De Camilli, P. (2010) Coupling between clathrin-dependent endocytic budding and F-BAR-dependent tubulation in a cell-free system. *Nature Cell Biology* **12**, 902-908
49. Pluen, A., Netti, P. A., Jain, R. K., and Berk, D. A. (1999) Diffusion of macromolecules in agarose gels: comparison of linear and globular configurations. *Biophysical journal* **77**, 542-552
50. Kelley, F. M., Favetta, B., Regy, R. M., Mittal, J., and Schuster, B. S. (2021) Amphiphilic proteins coassemble into multiphasic condensates and act as biomolecular surfactants. *Proceedings of the National Academy of Sciences* **118**, e2109967118
51. Yu, H., Lu, S., Gasior, K., Singh, D., Vazquez-Sanchez, S., Tapia, O., Toprani, D., Beccari, M. S., Yates, J. R., 3rd, Da Cruz, S., Newby, J. M., Lafarga, M., Gladfelter, A. S., Villa, E., and Cleveland, D. W. (2021) HSP70 chaperones RNA-free TDP-43 into anisotropic intranuclear liquid spherical shells. *Science* **371**

52. Garaizar, A., Espinosa, J. R., Joseph, J. A., Krainer, G., Shen, Y., Knowles, T. P. J., and Collepardo-Guevara, R. (2021) Intermolecular reorganisation of single-component condensates during ageing promotes multiphase architectures. *bioRxiv*, 2021.2010.2009.463670
53. Folkmann, A. W., Putnam, A., Lee, C. F., and Seydoux, G. (2021) Regulation of biomolecular condensates by interfacial protein clusters. *Science* **373**, 1218-1224
54. Suresh, S., and Edwardson, J. M. (2010) The Endophilin N-BAR Domain Perturbs the Structure of Lipid Bilayers. *Biochemistry* **49**, 5766-5771
55. Veatch, S. L., Machta, B. B., Shelby, S. A., Chiang, E. N., Holowka, D. A., and Baird, B. A. (2012) Correlation Functions Quantify Super-Resolution Images and Estimate Apparent Clustering Due to Over-Counting. *Plos One* **7**
56. Day, K. J., Kago, G., Wang, L. P., Richter, J. B., Hayden, C. C., Lafer, E. M., and Stachowiak, J. C. (2021) Liquid-like protein interactions catalyse assembly of endocytic vesicles. *Nature Cell Biology* **23**, 366-U113
57. Farsad, K., Ringstad, N., Takei, K., Floyd, S. R., Rose, K., and De Camilli, P. (2001) Generation of high curvature membranes mediated by direct endophilin bilayer interactions. *The Journal of cell biology* **155**, 193-200
58. Bergeron-Sandoval, L.-P., Kumar, S., Heris, H. K., Chang, C., Cornell, C. E., Keller, S. L., François, P., Hendricks, A. G., Ehrlicher, A. J., Pappu, R. V., and Michnick, S. W. (2021) Proteins with prion-like domains can form viscoelastic condensates that enable membrane remodeling and endocytosis. *bioRxiv*, 145664
59. Yuan, F., Alimohamadi, H., Bakka, B., Trementozzi, A. N., Day, K. J., Fawzi, N. L., Rangamani, P., and Stachowiak, J. C. (2021) Membrane bending by protein phase separation. *Proceedings of the National Academy of Sciences of the United States of America* **118**, 5A-6A
60. Rosendale, M., Van, T. N. N., Grillo-Bosch, D., Sposini, S., Claverie, L., Gauthereau, I., Claverol, S., Choquet, D., Sainlos, M., and Perrais, D. (2019) Functional recruitment of dynamin requires multimeric interactions for efficient endocytosis. *Nature communications* **10**, 1-14
61. Chen, Z., Chang, K., Capraro, B. R., Zhu, C., Hsu, C.-J., and Baumgart, T. (2014) Intradimer/Intermolecular interactions suggest autoinhibition mechanism in endophilin A1. *Journal of the American Chemical Society* **136**, 4557-4564
62. Zimmerman, S. B., and Trach, S. O. (1991) Estimation of macromolecule concentrations and excluded volume effects for the cytoplasm of Escherichia coli. *Journal of molecular biology* **222**, 599-620
63. Marsh, J. A., and Forman-Kay, J. D. (2010) Sequence determinants of compaction in intrinsically disordered proteins. *Biophysical journal* **98**, 2383-2390
64. Chen, Z., Zhu, C., Kuo, C. J., Robustelli, J., and Baumgart, T. (2016) The N-Terminal Amphipathic Helix of Endophilin Does Not Contribute to Its Molecular Curvature Generation Capacity. *J Am Chem Soc* **138**, 14616-14622

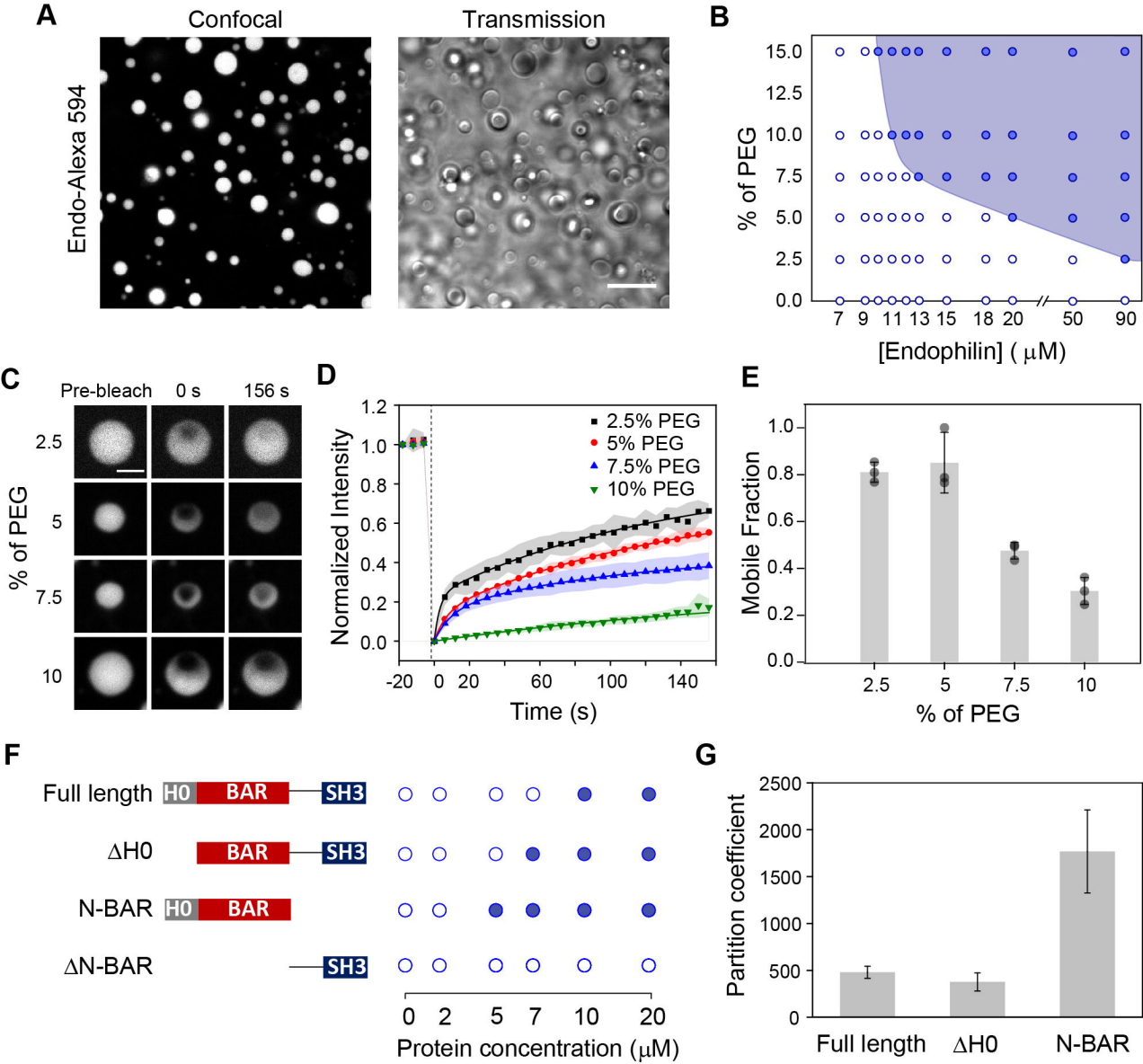
A
Confocal
Transmission
Endo-Alexa 594
B
% of PEG
15.0
12.5
10.0
7.5
5.0
2.5
0.0
7 9 11 13 15 18 20 50 90
[Endophilin] (μM)
C
Pre-bleach
0 s
156 s
% of PEG
2.5
5
7.5
10
D
Normalized Intensity
2.5% PEG
5% PEG
7.5% PEG
10% PEG
-20 0 20 60 100 140
Time (s)
E
Mobile Fraction
2.5 5 7.5 10
% of PEG
F
Full length
H0
BAR
SH3
ΔH0
N-BAR
ΔN-BAR
0 2 5 7 10 20
Protein concentration (μM)
G
Partition coefficient
Full length
ΔH0
N-BAR

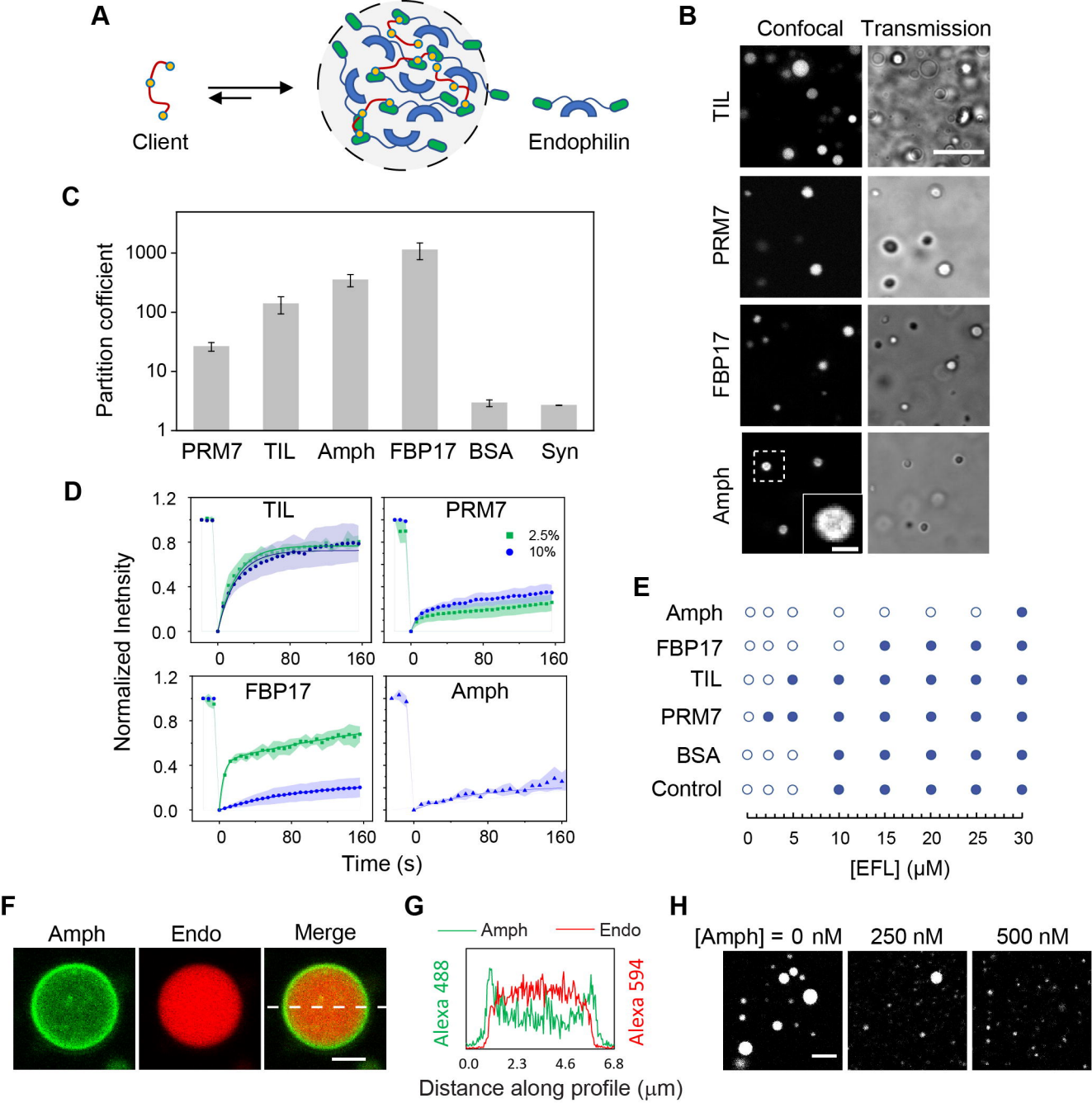
A
Client
Endophilin
B
Confocal
Transmission
TIL
PRM7
FBP17
Amph
C
Partition cofficient
1000
100
10
1
PRM7
TIL
Amph
FBP17
BSA
Syn
D
Normalized Inetnsity
TIL
PRM7
2.5%
10%
FBP17
Amph
1.2
0.8
0.4
0.0
0
80
160
Time (s)
E
Amph
FBP17
TIL
PRM7
BSA
Control
0
5
10
15
20
25
30
[EFL] (μM)
F
Amph
Endo
Merge
G
Amph
Endo
Alexa 488
Alexa 594
0.0
2.3
4.6
6.8
Distance along profile (μm)
H
[Amph] = 0 nM
250 nM
500 nM

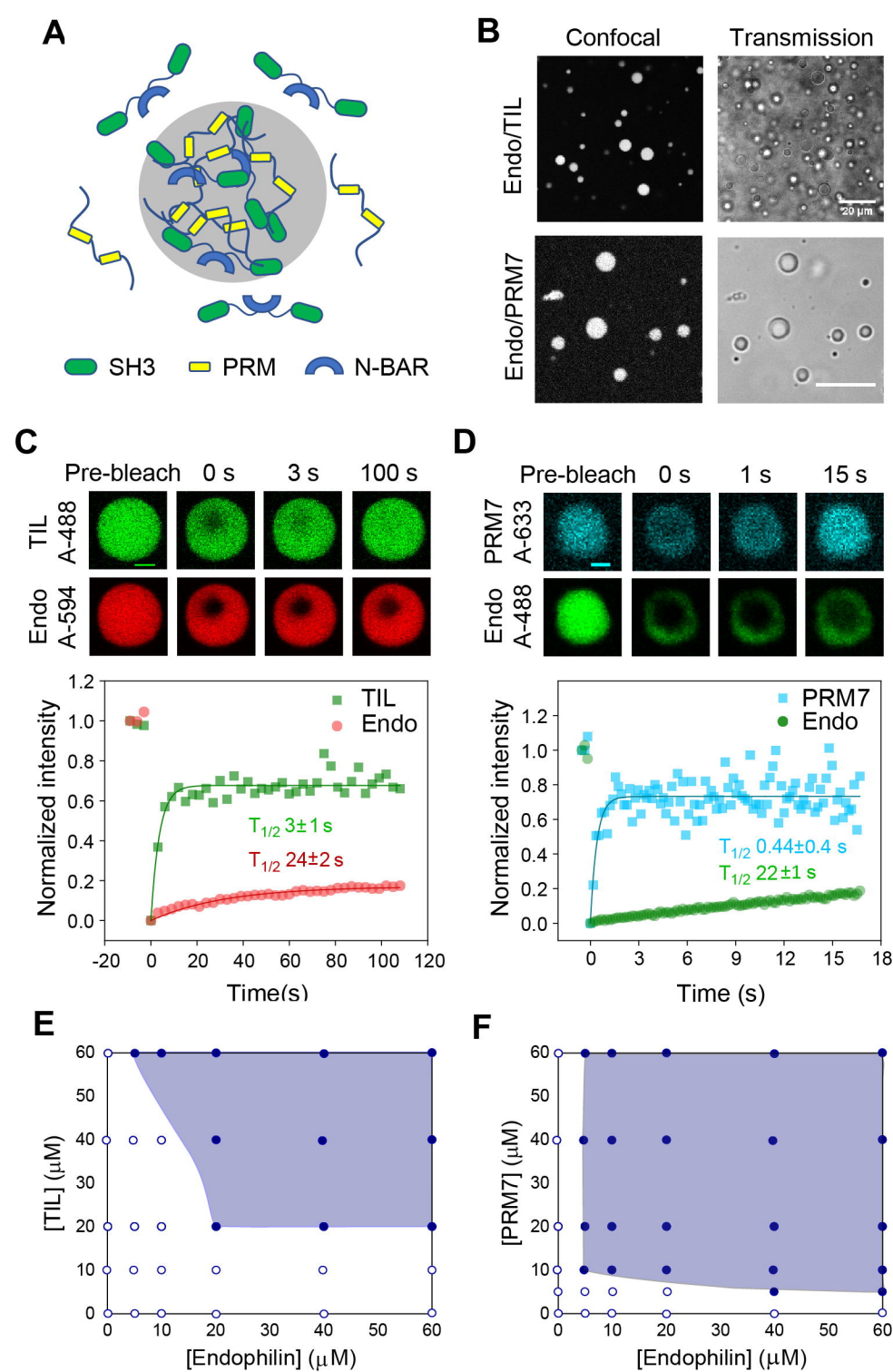
A
SH3
PRM
N-BAR
B
Confocal
Transmission
Endo/TIL
Endo/PRM7
20 µm
C
Pre-bleach
0 s
3 s
100 s
TIL A-488
Endo A-594
Normalized intensity
TIL
Endo
T1/2 3±1 s
T1/2 24±2 s
Time(s)
D
Pre-bleach
0 s
1 s
15 s
PRM7 A-633
Endo A-488
Normalized intensity
PRM7
Endo
T1/2 0.44±0.4 s
T1/2 22±1 s
Time (s)
E
[TIL] (µM)
[Endophilin] (µM)
F
[PRM7] (µM)
[Endophilin] (µM)

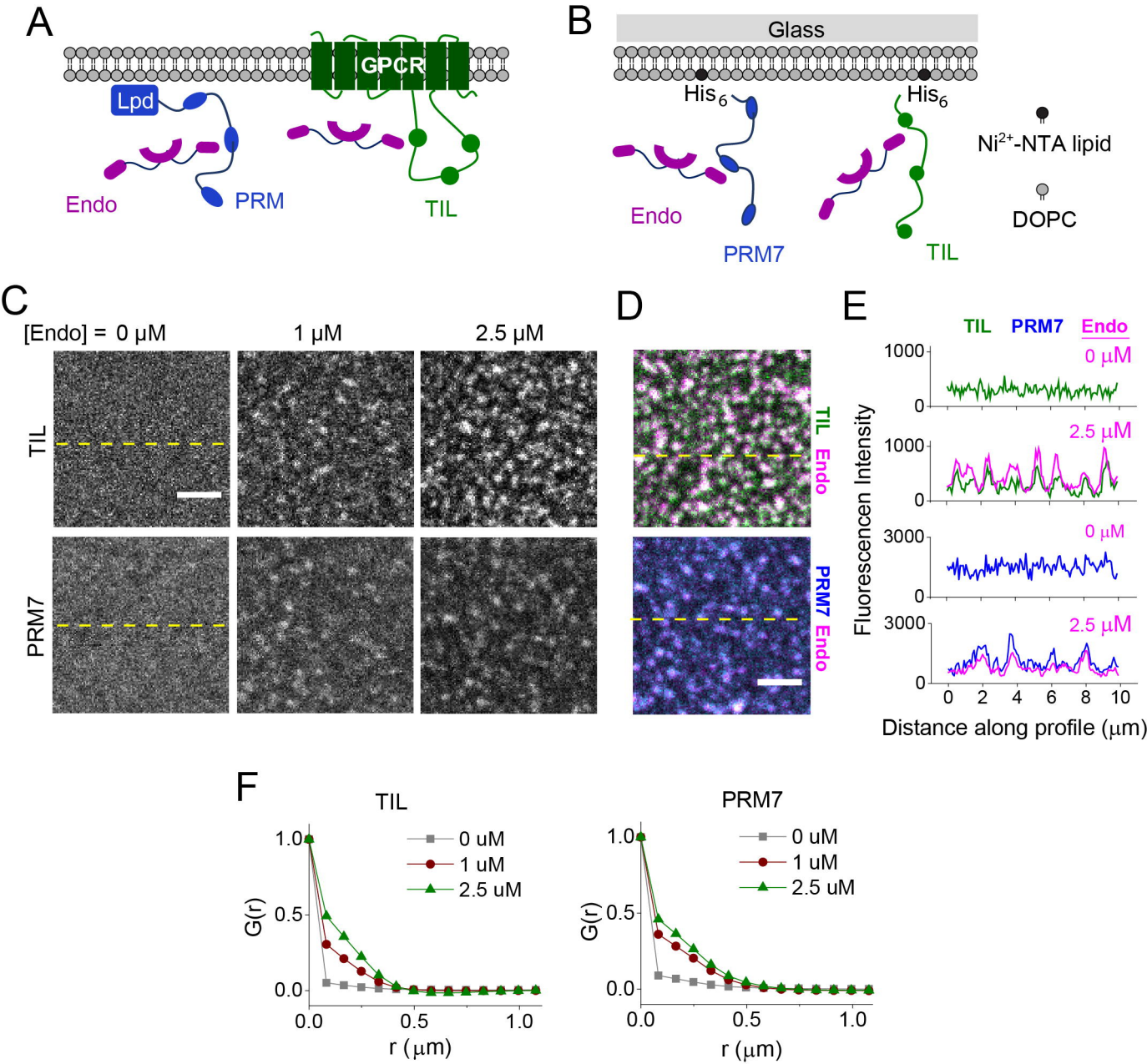
A
GPCR
Lpd
Endo
PRM
TIL
B
Glass
His6
His6
Ni2+-NTA lipid
DOPC
Endo
PRM7
TIL
C
[Endo] = 0 μM
1 μM
2.5 μM
TIL
PRM7
D
TIL Endo
PRM7 Endo
E
TIL PRM7 Endo
0 μM
2.5 μM
0 μM
2.5 μM
Fluorescencen Intensity
Distance along profile (μm)
F
TIL
PRM7
0 uM
1 uM
2.5 uM
G(r)
r (μm)

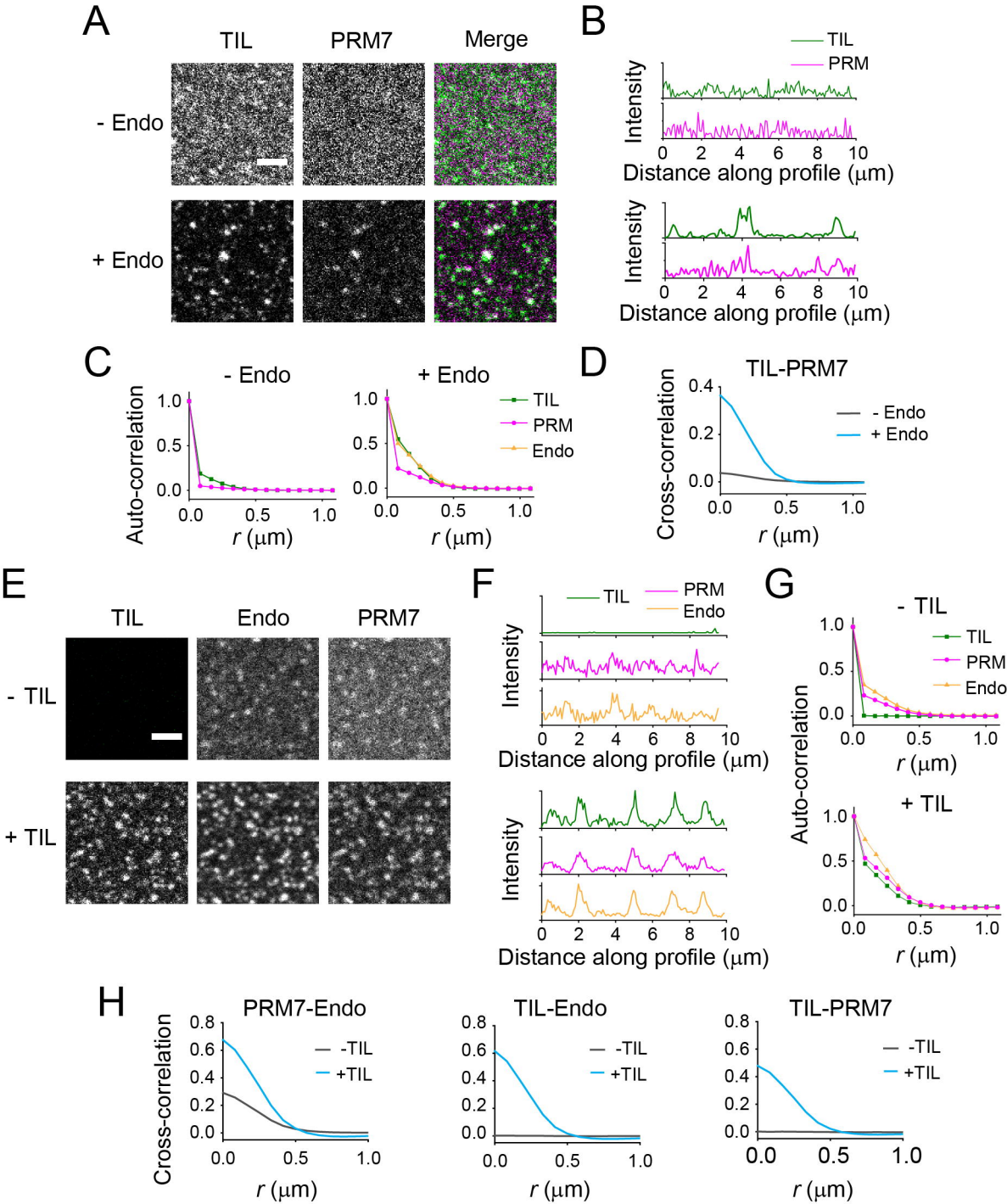
A
TIL
PRM7
Merge
- Endo
+ Endo
B
TIL
PRM
Intensity
0 2 4 6 8 10
Distance along profile (μm)
Intensity
0 2 4 6 8 10
Distance along profile (μm)
C
- Endo
+ Endo
Auto-correlation
1.0
0.5
0.0
0.0 0.5 1.0
r (μm)
TIL
PRM
Endo
D
TIL-PRM7
Cross-correlation
0.4
0.2
0.0
0.0 0.5 1.0
r (μm)
- Endo
+ Endo
E
TIL
Endo
PRM7
- TIL
+ TIL
F
TIL
PRM
Endo
Intensity
0 2 4 6 8 10
Distance along profile (μm)
Intensity
0 2 4 6 8 10
Distance along profile (μm)
G
- TIL
TIL
PRM
Endo
Auto-correlation
1.0
0.5
0.0
0.0 0.5 1.0
r (μm)
+ TIL
1.0
0.5
0.0
0.0 0.5 1.0
r (μm)
H
PRM7-Endo
TIL-Endo
TIL-PRM7
Cross-correlation
0.8
0.6
0.4
0.2
0.0
0.0 0.5 1.0
r (μm)
-TIL
+TIL

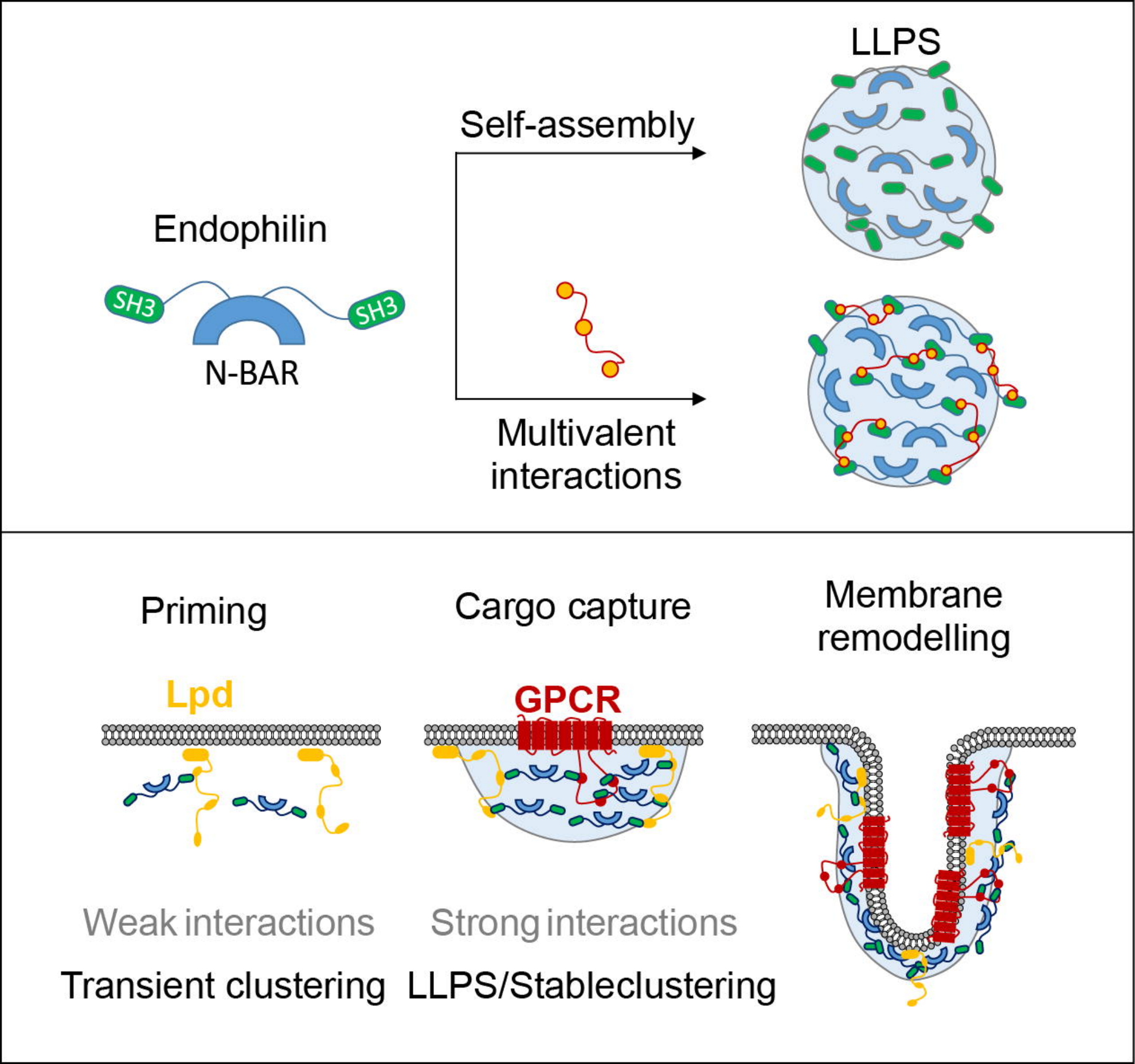
LLPS
Self-assembly
Endophilin
SH3
SH3
N-BAR
Multivalent
interactions
Priming
Cargo capture
Membrane
remodelling
Lpd
GPCR
Weak interactions
Strong interactions
Transient clustering
LLPS/Stableclustering